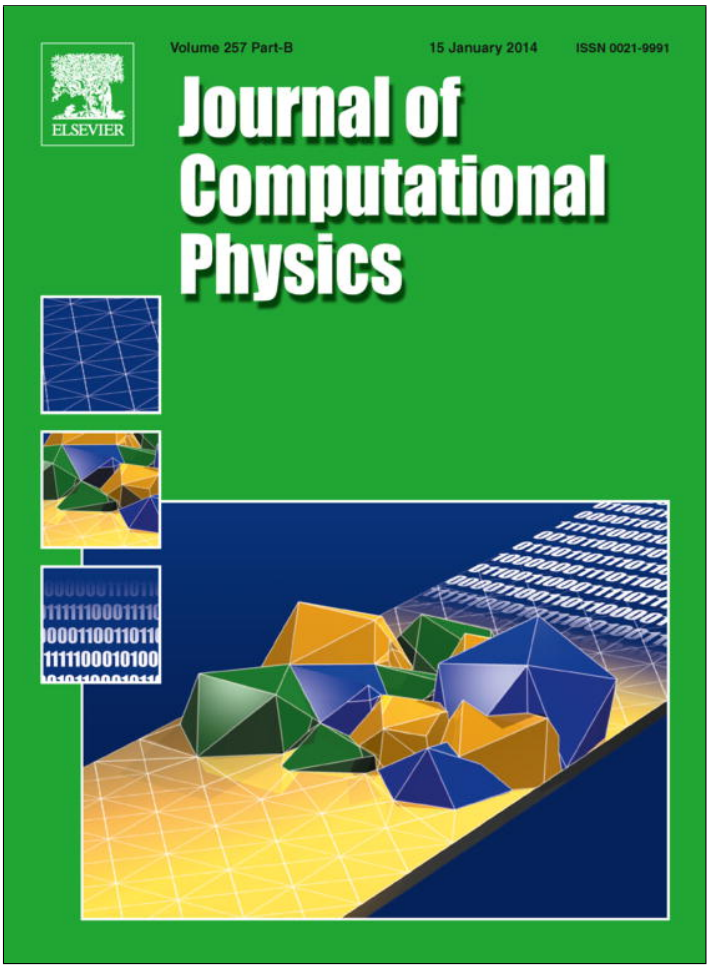

Journal of Computational Physics 257 (2014) 1321–1351

Contents lists available at ScienceDirect

Journal of Computational Physics

www.elsevier.com/locate/jcp

Error analysis of multipoint flux domain decomposition methods for evolutionary diffusion problems

A. Arrarás [a], L. Portero [a], I. Yotov [b,*]

[a] Departamento de Ingeniería Matemática e Informática, Universidad Pública de Navarra, Edificio de Las Encinas, Campus de Arrosadía, 31006 Pamplona, Spain

[b] Department of Mathematics, University of Pittsburgh, 301 Thackeray Hall, Pittsburgh, PA 15260, USA

ARTICLE INFO

Article history:
Received 2 August 2012
Received in revised form 1 June 2013
Accepted 4 August 2013
Available online 23 August 2013

Keywords:
Cell-centered finite difference
Domain decomposition
Fractional step
Mixed finite element
Multipoint flux approximation
Operator splitting

ABSTRACT

We study space and time discretizations for mixed formulations of parabolic problems. The spatial approximation is based on the multipoint flux mixed finite element method, which reduces to an efficient cell-centered pressure system on general grids, including triangles, quadrilaterals, tetrahedra, and hexahedra. The time integration is performed by using a domain decomposition time-splitting technique combined with multiterm fractional step diagonally implicit Runge–Kutta methods. The resulting scheme is unconditionally stable and computationally efficient, as it reduces the global system to a collection of uncoupled subdomain problems that can be solved in parallel without the need for Schwarz-type iteration. Convergence analysis for both the semidiscrete and fully discrete schemes is presented.

1. Introduction

Let us consider the parabolic initial-boundary value problem

$$p_t + \nabla \cdot \mathbf{u} = f \quad \text{in } \Omega \times (0,T], \tag{1a}$$

$$\mathbf{u} = -K\nabla p \quad \text{in } \Omega \times (0,T], \tag{1b}$$

$$p = g \quad \text{on } \Gamma_D \times (0,T], \tag{1c}$$

$$\mathbf{u}\cdot\mathbf{n} = 0 \quad \text{on } \Gamma_N \times (0,T], \tag{1d}$$

$$p = p_0 \quad \text{in } \Omega \times \{0\}, \tag{1e}$$

where $\Omega \subset \mathbb{R}^d$, $d = 2$ or 3, is a convex polygonal or polyhedral domain with Lipschitz continuous boundary $\partial\Omega = \overline{\Gamma}_D \cup \overline{\Gamma}_N$ such that $\Gamma_D \cap \Gamma_N = \emptyset$. In this formulation, $p = p(\mathbf{x},t)$, $\mathbf{u} = \mathbf{u}(\mathbf{x},t)$, $f = f(\mathbf{x},t)$, $g = g(\mathbf{x},t)$ and $p_0 = p_0(\mathbf{x})$. Further, $\mathbf{n}$ is the outward unit normal on $\partial\Omega$ and $K = K(\mathbf{x})$ is a symmetric and uniformly positive definite tensor satisfying, for some $0 < \kappa_* \leqslant \kappa^* < \infty$,

$$\kappa_* \xi^T \xi \leqslant \xi^T K(\mathbf{x}) \xi \leqslant \kappa^* \xi^T \xi \quad \forall \mathbf{x} \in \Omega,\ \forall \xi \in \mathbb{R}^d. \tag{2}$$

* Corresponding author.
E-mail address: yotov@math.pitt.edu (I. Yotov).

0021-9991/$ – see front matter
http://dx.doi.org/10.1016/j.jcp.2013.08.013

In applications to flow in porous media, $\mathbf{u}$ is the Darcy velocity, p is the fluid pressure, and K represents the rock permeability divided by the fluid viscosity.

In this work, we extend the formulation of the multipoint flux mixed finite element (MFMFE) method (cf. [1–7]) to time-dependent diffusion problems. In doing so, we introduce an unconditionally stable domain decomposition time-splitting technique which is designed to take advantage of the computational efficiency of parallel implementations. Similar ideas have been proposed in [8] and [9], where alternative compatible spatial discretizations – such as mimetic finite difference or expanded mixed finite element methods – have been studied in combination with fractional step time integrators. The convergence analysis developed in these works is restricted to the use of rectangular grids and diagonal tensors K. Here, we propose a general formulation which overcomes these restrictions and applies to two- and three-dimensional meshes composed of simplices, quadrilaterals and hexahedra, with full tensor coefficients.

The MFMFE scheme was motivated by the multipoint flux approximation (MPFA) methods (cf. [10–13]), where the introduction of sub-face (sub-edge in 2D) fluxes allows for local flux elimination and reduction to a cell-centered pressure scheme. In the MFMFE framework, similar elimination is achieved by employing appropriate finite element spaces and special quadrature rules. The MFMFE method is based on the lowest order Brezzi–Douglas–Marini, $\mathcal{BDM}_1$, or Brezzi–Douglas–Durán–Fortin, $\mathcal{BDDF}_1$, spaces (cf. [14] and [15], respectively), with a trapezoidal quadrature rule applied on the reference element (cf. [1,5–7]; see also [2–4] for an alternative formulation on quadrilateral grids using a broken Raviart–Thomas space).

The system of ordinary differential equations resulting from the spatial semidiscretization process is integrated in time by means of an operator splitting method (see [16]). To this end, the time derivative function is first partitioned via an overlapping domain decomposition splitting technique. This kind of splitting was first introduced in [17,18] in the context of regionally-additive schemes, and has been subsequently extended in [19–21] for solving linear parabolic problems. The monographs [22,23] show an overview of some recent contributions to the topic. As a matter of fact, the domain decomposition operator splitting requires a time integrator which allows for multiterm partitioning. A suitable choice for such a method can be found within the class of m-part fractional step Runge–Kutta (FSRK$_m$) schemes. These time integrators are constructed by merging together m diagonally implicit Runge–Kutta schemes into a single composite method. A survey on their use for solving linear parabolic problems can be found in [24]. Here, we present the general formulation of this class of schemes, and subsequently focus on a particular family of them, first proposed in [25], which extends the classical Peaceman–Rachford alternating direction implicit (ADI) method (cf. [26]) to a domain decomposition partitioning into an arbitrary number of terms. Similar combinations of the Peaceman–Rachford procedure with domain decomposition methods have been studied in [27]; however, the method there is based on non-overlapping decompositions in the context of elliptic problems and is restricted to an operator splitting into two split terms. For a related work on non-overlapping domain decompositions, see [28]. The key to the efficiency of our proposed method lies in reducing the system matrix to a collection of uncoupled submatrices of lower dimension. As compared to classical domain decomposition algorithms (cf. [29]), this technique does not involve any Schwarz iteration procedure, thus reducing the computational cost of the overall solution process.

We note that, to suitably merge the space and time discretization methods, the standard definition of the split functions for the scalar variable is no longer valid. In this case, we need to introduce a specific splitting for the flux variable that properly handles the degrees of freedom defined in the MFMFE approach.

We derive a priori error estimates for both the continuous-in-time and fully discrete formulations of the problem under study. Two variants of the MFMFE method are analyzed, namely: a symmetric scheme (cf. [1,2,4–6]), which applies to simplices and $\mathcal{O}(h^2)$-perturbations of parallelograms and parallelepipeds; and a non-symmetric method (cf. [3,7]), designed to preserve the accuracy on general quadrilaterals and hexahedra. The semidiscrete scheme is proved to satisfy the following convergence properties. In the symmetric case, the velocity and pressure variables are $\mathcal{O}(h)$ convergent, the latter being $\mathcal{O}(h^2)$ superconvergent at the cell centers. In the non-symmetric case, the velocity variable is shown to be $\mathcal{O}(h)$ convergent either when compared to a suitable projection of the true solution or when computed in a face-based (edge-based) norm; in turn, the pressure preserves its $\mathcal{O}(h)$ optimal convergence. After a suitable elimination procedure for the velocities, we obtain a fully discrete scheme in the pressure variable. The convergence analysis is described in detail for the symmetric method and just sketched for its non-symmetric counterpart. Based on stability and consistency results, unconditional convergence of order $\mathcal{O}(h+\tau^2)$ and superconvergence of order $\mathcal{O}(h^2+\tau^2)$ are obtained, respectively, in the continuous and discrete L^2-norm in space. These results extend those derived in [30] for the Peaceman–Rachford ADI method applied to linear problems to a domain decomposition splitting formula into an arbitrary number of split terms. From a computational viewpoint, parallel scalability tests for the non-iterative time-splitting technique are reported for the first time.

The rest of the paper is organized as follows. In Section 2, we describe the MFMFE semidiscrete scheme. Some convergence results for the elliptic problem are presented in Section 3. Based on these results, the error analysis is extended to the parabolic problem in Section 4. Section 5 introduces a domain decomposition splitting method leading to the fully discrete scheme. The convergence analysis for such a scheme is provided in Section 6. Finally, a series of numerical experiments illustrates the convergence and scalability behavior of the proposed algorithms in Section 7. A specific application to transient flow modeling in heterogeneous porous media is also discussed.

2. The multipoint flux mixed finite element method

In this section, we introduce an MFMFE formulation based on the $\mathcal{BDM}_1$ or $\mathcal{BDDF}_1$ spaces. This formulation is defined on simplicial, quadrilateral and hexahedral elements. The method further considers a suitable quadrature rule which allows for local velocity elimination, thus yielding a cell-centered semidiscrete scheme for the pressure. For the sake of completeness in the presentation, we provide some well-known expressions of finite element mappings and mixed finite element spaces for the type of elements under consideration.

2.1. The weak formulation

For a domain $G \subset \mathbb{R}^d$, let $W^{k,p}(G)$ be the standard Sobolev space, with $k \in \mathbb{R}$ and $1 \leqslant p \leqslant \infty$, endowed with the norm and seminorm $\|\cdot\|_{k,p,G}$ and $|\cdot|_{k,p,G}$, respectively. Let $H^k(G)$ be the Hilbert space $W^{k,2}(G)$, endowed with the norm and seminorm $\|\cdot\|_{k,G}$ and $|\cdot|_{k,G}$, respectively. We further denote by $(\cdot,\cdot)_G$ and $\|\cdot\|_G$ the inner product and norm, respectively, in either $L^2(G)$ or $(L^2(G))^d$. The subscript G will be omitted whenever $G = \Omega$. For a section of the domain or element boundary $S \subset \mathbb{R}^{d-1}$, $\langle\cdot,\cdot\rangle_S$ and $\|\cdot,\cdot\|_S$ represent the $L^2(S)$-inner product (or duality pairing) and norm, respectively. We shall also use the space

$$H(\mathrm{div}; G) = \left\{\mathbf{v} \in \left(L^2(G)\right)^d \colon \nabla\cdot\mathbf{v} \in L^2(G)\right\},$$

with corresponding norm

$$\|\mathbf{v}\|_{\mathrm{div};G} = \left(\|\mathbf{v}\|_G^2 + \|\nabla\cdot\mathbf{v}\|_G^2\right)^{1/2}.$$

Finally, if $\chi \equiv \chi(G)$ denotes any of the above normed spaces on G, with associated norm $\|\cdot\|_\chi$, we shall consider $L^q([0,T];\chi)$ as the space of χ-valued functions $\varphi : [0,T] \to \chi(G)$, equipped with the norm

$$\|\varphi\|_{L^q([0,T];\chi)} \equiv \|\varphi\|_{L^q(\chi)} = \begin{cases} \left(\int_0^T \|\varphi(t)\|_\chi^q \, dt\right)^{1/q} & \text{if } 1 \leqslant q < \infty, \\ \operatorname{ess\,sup}_{t\in[0,T]} \|\varphi(t)\|_\chi & \text{if } q = \infty. \end{cases}$$

In this framework, the variational formulation of the first-order system (1) is given by: *Find* $(\mathbf{u}, p) : [0,T] \to H_0(\mathrm{div};\Omega) \times L^2(\Omega)$ *such that*

$$(p_t, w) + (\nabla\cdot\mathbf{u}, w) = (f, w) \qquad \forall w \in L^2(\Omega), \tag{3a}$$

$$\left(K^{-1}\mathbf{u}, \mathbf{v}\right) = (p, \nabla\cdot\mathbf{v}) - \langle g, \mathbf{v}\cdot\mathbf{n}\rangle_{\Gamma_D} \qquad \forall \mathbf{v} \in H_0(\mathrm{div};\Omega), \tag{3b}$$

$$p(0) = p_0, \tag{3c}$$

where

$$H_0(\mathrm{div};\Omega) = \left\{\mathbf{v} \in H(\mathrm{div};\Omega) \colon \mathbf{v}\cdot\mathbf{n} = 0 \text{ on } \Gamma_N\right\}.$$

2.2. Finite element mappings

Let $\mathcal{T}_h$ be a conforming, shape-regular and quasi-uniform partition of Ω, where $h = \max_{E\in\mathcal{T}_h} \mathrm{diam}(E)$. The elements are considered to be triangles or convex quadrilaterals, in two dimensions, and tetrahedra or convex hexahedra, in three dimensions. For any $E \in \mathcal{T}_h$, there exists a bijection mapping $F_E : \hat{E} \to E$, where $\hat{E}$ is the reference element. We denote by DF_E the Jacobian matrix of the transformation and let $J_E = |\det(DF_E)|$. In addition, we consider the inverse mapping F_E^{-1} and obtain its Jacobian matrix to be $DF_E^{-1}(\mathbf{x}) = (DF_E(\hat{\mathbf{x}}))^{-1}$ with determinant $J_E^{-1}(\mathbf{x}) = 1/J_E(\hat{\mathbf{x}})$. In the sequel, we describe in detail how F_E is constructed for the three-dimensional instances.

In the case of tetrahedra, $\hat{E}$ is the reference tetrahedron with vertices $\hat{\mathbf{r}}_1 = (0,0,0)^T$, $\hat{\mathbf{r}}_2 = (1,0,0)^T$, $\hat{\mathbf{r}}_3 = (0,1,0)^T$ and $\hat{\mathbf{r}}_4 = (0,0,1)^T$. Let $\mathbf{r}_i = (x_i, y_i, z_i)^T$ be the corresponding vertices of E, for $i = 1,2,3,4$. The outward unit normal vectors to the faces of $\hat{E}$ and E are denoted by $\hat{\mathbf{n}}_i$ and $\mathbf{n}_i$, respectively, for $i = 1,2,3,4$. We shall also use the notation $\hat{\mathbf{n}}_{\hat{e}}$ and $\mathbf{n}_e$ to represent the outward unit normals on faces $\hat{e} \subset \partial\hat{E}$ and $e \subset \partial E$, respectively. The affine mapping F_E is given, for any $\hat{\mathbf{x}} = (\hat{x}, \hat{y}, \hat{z})^T \in \hat{E}$, by

$$F_E(\hat{\mathbf{x}}) = \mathbf{r}_1(1 - \hat{x} - \hat{y} - \hat{z}) + \mathbf{r}_2\hat{x} + \mathbf{r}_3\hat{y} + \mathbf{r}_4\hat{z}. \tag{4}$$

The Jacobian matrix of F_E is thus

$$DF_E = [\mathbf{r}_{21}, \mathbf{r}_{31}, \mathbf{r}_{41}],$$

where $\mathbf{r}_{ij} = \mathbf{r}_i - \mathbf{r}_j$, and its determinant is $J_E = 6|E|$, $|E|$ being the volume of E.

In the case of hexahedra, $\hat{E}$ denotes the unit cube with vertices $\hat{\mathbf{r}}_1 = (0,0,0)^T$, $\hat{\mathbf{r}}_2 = (1,0,0)^T$, $\hat{\mathbf{r}}_3 = (1,1,0)^T$, $\hat{\mathbf{r}}_4 = (0,1,0)^T$, $\hat{\mathbf{r}}_5 = (0,0,1)^T$, $\hat{\mathbf{r}}_6 = (1,0,1)^T$, $\hat{\mathbf{r}}_7 = (1,1,1)^T$ and $\hat{\mathbf{r}}_8 = (0,1,1)^T$. Let $\mathbf{r}_i$ be the corresponding vertices of E, for

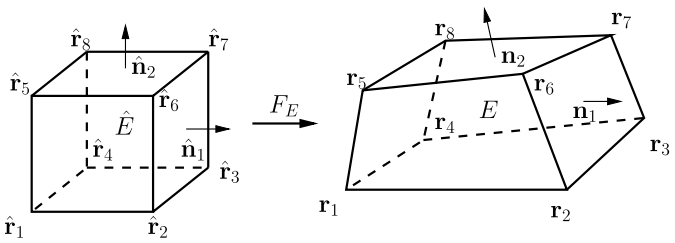

Fig. 1. Trilinear hexahedral mapping.

$i = 1, 2, \ldots, 8$, as shown in Fig. 1. Note that the hexahedra may have non-planar faces. In this case, F_E is a trilinear mapping of the form

$$\begin{aligned} F_E(\hat{\mathbf{x}}) = {} & \mathbf{r}_1(1-\hat{x})(1-\hat{y})(1-\hat{z}) + \mathbf{r}_2\hat{x}(1-\hat{y})(1-\hat{z}) + \mathbf{r}_3\hat{x}\hat{y}(1-\hat{z}) + \mathbf{r}_4(1-\hat{x})\hat{y}(1-\hat{z}) \\ & + \mathbf{r}_5(1-\hat{x})(1-\hat{y})\hat{z} + \mathbf{r}_6\hat{x}(1-\hat{y})\hat{z} + \mathbf{r}_7\hat{x}\hat{y}\hat{z} + \mathbf{r}_8(1-\hat{x})\hat{y}\hat{z}. \end{aligned}$$

Rearranging terms, it can be expressed as

$$\begin{aligned} F_E(\hat{\mathbf{x}}) = {} & \mathbf{r}_1 + \mathbf{r}_{21}\hat{x} + \mathbf{r}_{41}\hat{y} + \mathbf{r}_{51}\hat{z} + (\mathbf{r}_{34} - \mathbf{r}_{21})\hat{x}\hat{y} + (\mathbf{r}_{65} - \mathbf{r}_{21})\hat{x}\hat{z} \\ & + (\mathbf{r}_{85} - \mathbf{r}_{41})\hat{y}\hat{z} + (\mathbf{r}_{21} - \mathbf{r}_{34} - \mathbf{r}_{65} + \mathbf{r}_{78})\hat{x}\hat{y}\hat{z}. \end{aligned} \tag{5}$$

Given F_E, each component of the Jacobian matrix is a bilinear function of two space variables, i.e.,

$$\begin{aligned} DF_E(\hat{\mathbf{x}}) = \big[& \mathbf{r}_{21} + (\mathbf{r}_{34} - \mathbf{r}_{21})\hat{y} + (\mathbf{r}_{65} - \mathbf{r}_{21})\hat{z} + (\mathbf{r}_{21} - \mathbf{r}_{34} - \mathbf{r}_{65} + \mathbf{r}_{78})\hat{y}\hat{z}, \\ & \mathbf{r}_{41} + (\mathbf{r}_{34} - \mathbf{r}_{21})\hat{x} + (\mathbf{r}_{85} - \mathbf{r}_{41})\hat{z} + (\mathbf{r}_{21} - \mathbf{r}_{34} - \mathbf{r}_{65} + \mathbf{r}_{78})\hat{x}\hat{z}, \\ & \mathbf{r}_{51} + (\mathbf{r}_{65} - \mathbf{r}_{21})\hat{x} + (\mathbf{r}_{85} - \mathbf{r}_{41})\hat{y} + (\mathbf{r}_{21} - \mathbf{r}_{34} - \mathbf{r}_{65} + \mathbf{r}_{78})\hat{x}\hat{y} \big]. \end{aligned}$$

In the cases of triangles and convex quadrilaterals, the mappings are two-dimensional counterparts of (4) and (5), respectively (see, e.g., [1]).

To conclude, considering the previous mappings and the classical formula $\nabla\phi = DF_E^{-T}\hat{\nabla}\hat{\phi}$, where $\phi(\mathbf{x}) = \hat{\phi}(\hat{\mathbf{x}})$, it holds that

$$\mathbf{n}_i = \frac{DF_E^{-T}\hat{\mathbf{n}}_i}{|DF_E^{-T}\hat{\mathbf{n}}_i|_{\mathbb{R}^d}}, \tag{6}$$

on any face or edge $e_i \subset \partial E$, where $|\cdot|_{\mathbb{R}^d}$ stands for the Euclidean norm in $\mathbb{R}^d$ and the superscript $-T$ denotes inversion and transposition.

2.3. Mixed finite element spaces

Let $\hat{V}(\hat{E})$ and $\hat{W}(\hat{E})$ be the finite element spaces on the reference element $\hat{E}$. For simplicial elements, we use the $\mathcal{BDM}_1$ spaces on the unit triangle and the $\mathcal{BDDF}_1$ spaces on the unit tetrahedron, i.e.,

$$\hat{V}(\hat{E}) = \big(\mathbb{P}_1(\hat{E})\big)^d, \qquad \hat{W}(\hat{E}) = \mathbb{P}_0(\hat{E}),$$

where $\mathbb{P}_k$ denotes the space of polynomials of degree not greater than k. On the unit square, we define $\mathcal{BDM}_1$ spaces of the form

$$\hat{V}(\hat{E}) = \big(\mathbb{P}_1(\hat{E})\big)^2 + r\,\mathrm{curl}\big(\hat{x}^2\hat{y}\big) + s\,\mathrm{curl}\big(\hat{x}\hat{y}^2\big), \qquad \hat{W}(\hat{E}) = \mathbb{P}_0(\hat{E}),$$

where r and s are real constants. Finally, on the unit cube, we use the so-called enhanced $\mathcal{BDDF}_1$ spaces introduced in [5]:

$$\begin{aligned} \hat{V}(\hat{E}) = {} & \mathcal{BDDF}_1(\hat{E}) + r_2\,\mathrm{curl}\big(0, 0, \hat{x}^2\hat{z}\big)^T + r_3\,\mathrm{curl}\big(0, 0, \hat{x}^2\hat{y}\hat{z}\big)^T + s_2\,\mathrm{curl}\big(\hat{x}\hat{y}^2, 0, 0\big)^T + s_3\,\mathrm{curl}\big(\hat{x}\hat{y}^2\hat{z}, 0, 0\big)^T \\ & + t_2\,\mathrm{curl}\big(0, \hat{y}\hat{z}^2, 0\big)^T + t_3\,\mathrm{curl}\big(0, \hat{x}\hat{y}\hat{z}^2, 0\big)^T, \\ \hat{W}(\hat{E}) = {} & \mathbb{P}_0(\hat{E}), \end{aligned}$$

where the $\mathcal{BDDF}_1(\hat{E})$ space is given by

$$\begin{aligned} \mathcal{BDDF}_1(\hat{E}) = {} & \big(\mathbb{P}_1(\hat{E})\big)^3 + r_0\,\mathrm{curl}(0, 0, \hat{x}\hat{y}\hat{z})^T + r_1\,\mathrm{curl}\big(0, 0, \hat{x}\hat{y}^2\big)^T + s_0\,\mathrm{curl}(\hat{x}\hat{y}\hat{z}, 0, 0)^T + s_1\,\mathrm{curl}\big(\hat{y}\hat{z}^2, 0, 0\big)^T \\ & + t_0\,\mathrm{curl}(0, \hat{x}\hat{y}\hat{z}, 0)^T + t_1\,\mathrm{curl}\big(0, \hat{x}^2\hat{z}, 0\big)^T, \end{aligned}$$

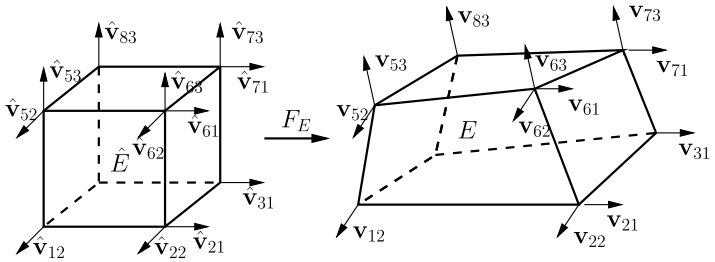

Fig. 2. Degrees of freedom and basis functions for the enhanced $\mathcal{BDDF}_1$ velocity space on hexahedra.

r_i, s_i and t_i being real constants, for $i = 0, 1, 2, 3$. Note that, in all four cases, $\hat{\nabla} \cdot \hat{V}(\hat{E}) = \hat{W}(\hat{E})$. Furthermore, on any face (edge in 2D) $\hat{e} \subset \partial \hat{E}$, $\hat{\mathbf{v}} \in \hat{V}(\hat{E})$ is such that $\hat{\mathbf{v}} \cdot \hat{\mathbf{n}}_{\hat{e}} \in \mathbb{P}_1(\hat{e})$ on the reference simplex or the reference square, and $\hat{\mathbf{v}} \cdot \hat{\mathbf{n}}_{\hat{e}} \in \mathbb{Q}_1(\hat{e})$ on the reference cube. Here, $\mathbb{Q}_1(\hat{e})$ denotes the space of bilinear functions on $\hat{e}$. The degrees of freedom for $\hat{\mathbf{v}} \in \hat{V}(\hat{E})$ are chosen to be the values of $\hat{\mathbf{v}} \cdot \hat{\mathbf{n}}_{\hat{e}}$ at the vertices of each face (edge) $\hat{e}$; see Fig. 2 for the hexahedral case.

The spaces $V(E)$ and $W(E)$ on any physical element $E \in \mathcal{T}_h$ are defined via the transformations

$$\mathbf{v} \leftrightarrow \hat{\mathbf{v}} : \mathbf{v} = \left(\frac{1}{J_E} DF_E \hat{\mathbf{v}} \right) \circ F_E^{-1}, \qquad w \leftrightarrow \hat{w} : w = \hat{w} \circ F_E^{-1}.$$

Note that any $\mathbf{v} \in V(E)$ is obtained from the corresponding $\hat{\mathbf{v}} \in \hat{V}(\hat{E})$ through the Piola transformation (cf. [31]). This transformation preserves the continuity of the normal components of the velocity vectors across interelement faces (edges), which is a necessary condition for building approximations to $H(\mathrm{div}; \Omega)$. More precisely, we have (cf. [32])

$$(\nabla \cdot \mathbf{v}, w)_E = (\hat{\nabla} \cdot \hat{\mathbf{v}}, \hat{w})_{\hat{E}}, \qquad \langle \mathbf{v} \cdot \mathbf{n}_e, w \rangle_e = \langle \hat{\mathbf{v}} \cdot \hat{\mathbf{n}}_{\hat{e}}, \hat{w} \rangle_{\hat{e}}, \tag{7}$$

where $(\mathbf{v}, w) \in V(E) \times W(E)$ and $(\hat{\mathbf{v}}, \hat{w}) \in \hat{V}(\hat{E}) \times \hat{W}(\hat{E})$. Moreover, (6) implies that

$$\mathbf{v} \cdot \mathbf{n}_e = \left(\frac{1}{|J_E DF_E^{-T} \hat{\mathbf{n}}_{\hat{e}}|_{\mathbb{R}^d}} \hat{\mathbf{v}} \cdot \hat{\mathbf{n}}_{\hat{e}} \right) \circ F_E^{-1}(\mathbf{x}),$$

and (7) implies that

$$\nabla \cdot \mathbf{v} = \left(\frac{1}{J_E} \hat{\nabla} \cdot \hat{\mathbf{v}} \right) \circ F_E^{-1}(\mathbf{x}).$$

For any $\mathbf{v} \in V(E)$, while J_E is constant on simplices, this is not true on quadrilaterals and hexahedra. As a result, $\nabla \cdot \mathbf{v}$ is not constant in the latter cases. Along these lines, $\mathbf{v} \cdot \mathbf{n}_e \in \mathbb{P}_1(e)$ on simplices and quadrilaterals, but $\mathbf{v} \cdot \mathbf{n}_e \notin \mathbb{Q}_1(e)$ on hexahedra.

Finally, the global MFE spaces $V_h \times W_h \subset H_0(\mathrm{div}; \Omega) \times L^2(\Omega)$ on $\mathcal{T}_h$ are given by

$$V_h = \left\{ \mathbf{v} \in H_0(\mathrm{div}; \Omega) \colon \mathbf{v}|_E \leftrightarrow \hat{\mathbf{v}},\ \hat{\mathbf{v}} \in \hat{V}(\hat{E})\ \forall E \in \mathcal{T}_h \right\},$$
$$W_h = \left\{ w \in L^2(\Omega) \colon w|_E \leftrightarrow \hat{w},\ \hat{w} \in \hat{W}(\hat{E})\ \forall E \in \mathcal{T}_h \right\}.$$

As we shall see below, a proper definition of the semidiscrete scheme requires the non-homogeneous Dirichlet boundary data to be projected onto the lowest order Raviart–Thomas ($\mathcal{RT}_0$) velocity space. Let us recall that the $\mathcal{RT}_0$ spaces, as defined in [33,34], are given by

$$\hat{V}^0(\hat{E}) = \begin{pmatrix} r_1 + s\hat{x} \\ r_2 + s\hat{y} \\ r_3 + s\hat{z} \end{pmatrix}, \qquad \hat{W}^0(\hat{E}) = \mathbb{P}_0(\hat{E}),$$

and

$$\hat{V}^0(\hat{E}) = \begin{pmatrix} r_1 + s_1\hat{x} \\ r_2 + s_2\hat{y} \\ r_3 + s_3\hat{z} \end{pmatrix}, \qquad \hat{W}^0(\hat{E}) = \mathbb{P}_0(\hat{E}),$$

on the reference tetrahedron and the reference cube, respectively, where r_i, s_i and s, for $i = 1, 2, 3$, are constants. The definition of the $\mathcal{RT}_0$ spaces on two-dimensional elements is analogous.

In this case, $\hat{\nabla} \cdot \hat{V}^0(\hat{E}) = \hat{W}^0(\hat{E})$ and $\hat{\mathbf{v}} \cdot \hat{\mathbf{n}}_{\hat{e}} \in \mathbb{P}_0(\hat{e})$. The degrees of freedom for $\hat{\mathbf{v}} \in \hat{V}^0(\hat{E})$ are chosen to be the values of $\hat{\mathbf{v}} \cdot \hat{\mathbf{n}}_{\hat{e}}$ at the midpoints of each face (edge) $\hat{e} \subset \partial \hat{E}$. The global spaces $V_h^0 \times W_h^0 \subset H_0(\mathrm{div}; \Omega) \times L^2(\Omega)$ on $\mathcal{T}_h$ are defined in accordance with $V_h \times W_h$. By definition, $V_h^0 \subset V^h$ and $W_h^0 = W^h$.

2.4. Projection operators

Let us now recall how to construct the projection operator onto the space V_h. We first introduce a reference element projection operator $\hat{\Pi} : (H^1(\hat{E}))^d \to \hat{V}(\hat{E})$, which is defined, for any $\hat{\mathbf{q}} \in (H^1(\hat{E}))^d$, as

$$\left\langle (\hat{\Pi}\hat{\mathbf{q}} - \hat{\mathbf{q}}) \cdot \hat{\mathbf{n}}_{\hat{e}}, \hat{q}_1 \right\rangle = 0,$$

on any face (edge) $\hat{e} \subset \partial\hat{E}$, where $\hat{q}_1 \in \mathbb{P}_1(\hat{e})$ if $\hat{E}$ is the unit simplex or the unit square, and $\hat{q}_1 \in \mathbb{Q}_1(\hat{e})$ if $\hat{E}$ is the unit cube. Then, the global projection operator $\Pi_h : (H^1(\Omega))^d \cap H_0(\mathrm{div};\Omega) \to V_h$ is locally defined on each element E via the Piola transformation, i.e., for any $\mathbf{q} \in (H^1(\Omega))^d \cap H_0(\mathrm{div};\Omega)$,

$$\Pi_h \mathbf{q}|_E \leftrightarrow \widehat{\Pi_h \mathbf{q}}, \qquad \widehat{\Pi_h \mathbf{q}} = \hat{\Pi}\hat{\mathbf{q}} \in \hat{V}(\hat{E}).$$

Based on the previous expressions, it can be deduced that

$$\left(\nabla \cdot (\Pi_h \mathbf{q} - \mathbf{q}), w\right) = 0 \quad \forall w \in W_h.$$

The idea is analogous for the $\mathcal{RT}_0$ space V_h^0. The reference element projection operator $\hat{\Pi}^0 : (H^1(\hat{E}))^d \to \hat{V}^0(\hat{E})$ is defined, for any $\hat{\mathbf{q}} \in (H^1(\hat{E}))^d$, as

$$\left\langle \left(\hat{\Pi}^0\hat{\mathbf{q}} - \hat{\mathbf{q}}\right) \cdot \hat{\mathbf{n}}_{\hat{e}}, \hat{q}_0 \right\rangle = 0,$$

on any face (edge) $\hat{e} \subset \partial\hat{E}$, where $\hat{q}_0 \in \mathbb{P}_0(\hat{e})$. Then, the global projection operator $\Pi_h^0 : (H^1(\Omega))^d \cap H_0(\mathrm{div};\Omega) \to V_h^0$ is obtained similarly to the case of Π_h. As a result, it also satisfies, for any $\mathbf{q} \in (H^1(\Omega))^d \cap H_0(\mathrm{div};\Omega)$,

$$\left(\nabla \cdot \left(\Pi_h^0 \mathbf{q} - \mathbf{q}\right), w\right) = 0 \quad \forall w \in W_h^0.$$

Finally, we also require the standard $L^2(\Omega)$-projection operator onto the space W_h. To define it, we first introduce the $L^2(\hat{E})$-projection $\hat{\mathcal{P}} : L^2(\hat{E}) \to \hat{W}(\hat{E})$ satisfying, for any $\hat{\varphi} \in \hat{W}(\hat{E})$,

$$(\hat{\varphi} - \hat{\mathcal{P}}\hat{\varphi}, \hat{w})_{\hat{E}} = 0 \quad \forall \hat{w} \in \hat{W}(\hat{E}).$$

Then, we let $\mathcal{P}_h : L^2(\Omega) \to W_h$ be the $L^2(\Omega)$-projection operator, which is locally defined on each element E, for any $\varphi \in L^2(\Omega)$, as

$$\mathcal{P}_h \varphi|_E = \hat{\mathcal{P}}\hat{\varphi} \circ F_E^{-1}.$$

It is not difficult to see that, due to (7),

$$(\varphi - \mathcal{P}_h\varphi, \nabla \cdot \mathbf{v}) = 0 \quad \forall \mathbf{v} \in V_h. \tag{8}$$

2.5. Quadrature rules

When discretizing the mixed variational formulation (3), it is necessary to compute an integral of the form $(K^{-1}\mathbf{q}, \mathbf{v})$, for $\mathbf{q}, \mathbf{v} \in V_h$, which derives from (3b). In doing so, the MFMFE method considers a quadrature rule that permits to reduce the semidiscrete problem to a cell-centered finite difference scheme for the pressure. The integration on each element $E \in \mathcal{T}_h$ is accomplished by mapping to the reference element $\hat{E}$, where the quadrature rule is defined. Namely, for any $\mathbf{q}, \mathbf{v} \in V_h$ and $\hat{\mathbf{q}}, \hat{\mathbf{v}} \in \hat{V}(\hat{E})$,

$$\left(K^{-1}\mathbf{q}, \mathbf{v}\right)_E = \left(\frac{1}{J_E} DF_E^T K^{-1}\left(F_E(\hat{\mathbf{x}})\right) DF_E \hat{\mathbf{q}}, \hat{\mathbf{v}}\right)_{\hat{E}} \equiv \left(\mathcal{K}_E^{-1}\hat{\mathbf{q}}, \hat{\mathbf{v}}\right)_{\hat{E}},$$

where

$$\mathcal{K}_E^{-1}(\hat{\mathbf{x}}) = \frac{1}{J_E(\hat{\mathbf{x}})} DF_E^T(\hat{\mathbf{x}}) K^{-1}\left(F_E(\hat{\mathbf{x}})\right) DF_E(\hat{\mathbf{x}}). \tag{9}$$

The quadrature rule on $E \in \mathcal{T}_h$ is given by the trapezoidal rule, i.e.,

$$\left(K^{-1}\mathbf{q}, \mathbf{v}\right)_{Q,E} \equiv \left(\mathcal{K}_E^{-1}\hat{\mathbf{q}}, \hat{\mathbf{v}}\right)_{\hat{Q},\hat{E}} \equiv \frac{|\hat{E}|}{n_v} \sum_{i=1}^{n_v} \mathcal{K}_E^{-1}(\hat{\mathbf{r}}_i)\hat{\mathbf{q}}(\hat{\mathbf{r}}_i) \cdot \hat{\mathbf{v}}(\hat{\mathbf{r}}_i),$$

where $|\hat{E}|$ is the volume (area) of $\hat{E}$ and n_v denotes the number of vertices of $\hat{E}$ (i.e., $n_v = 3$ for the unit triangle, $n_v = 4$ for the unit square or the unit tetrahedron and $n_v = 8$ for the unit cube). Hence, the global quadrature rule is defined as

$$\left(K^{-1}\mathbf{q},\mathbf{v}\right)_Q \equiv \sum_{E\in\mathcal{T}_h}\left(K^{-1}\mathbf{q},\mathbf{v}\right)_{Q,E}. \tag{10}$$

Mapping back to the physical element E, we obtain

$$\left(K^{-1}\mathbf{q},\mathbf{v}\right)_{Q,E} = \frac{1}{n_v}\sum_{i=1}^{n_v} J_E(\hat{\mathbf{r}}_i)K^{-1}(\mathbf{r}_i)\mathbf{q}(\mathbf{r}_i)\cdot\mathbf{v}(\mathbf{r}_i). \tag{11}$$

If the mesh is composed of highly distorted quadrilateral or hexahedra, we modify formula (9) to get

$$\tilde{\mathcal{K}}_E^{-1}(\hat{\mathbf{x}}) = \frac{1}{J_E(\hat{\mathbf{x}})}DF_E^T(\hat{\mathbf{x}}_c)\overline{K}_E^{-1}DF_E(\hat{\mathbf{x}}),$$

where $\overline{K}_E$ is a constant matrix such that $(\overline{K}_E)_{ij}$ is the mean value of $(K)_{ij}$ on E, $(\overline{K}_E)_{ij}$ and $(K)_{ij}$ being the elements on the ith row and jth column of matrices $\overline{K}_E$ and K, respectively. Furthermore, $\hat{\mathbf{x}}_c$ denotes the center of mass of $\hat{E}$. In this case, the quadrature rule on $E\in\mathcal{T}_h$ takes the form

$$\left(K^{-1}\mathbf{q},\mathbf{v}\right)_{Q,E} \equiv \left(\tilde{\mathcal{K}}_E^{-1}\hat{\mathbf{q}},\hat{\mathbf{v}}\right)_{\hat{Q},\hat{E}} \equiv \frac{|\hat{E}|}{n_v}\sum_{i=1}^{n_v}\tilde{\mathcal{K}}_E^{-1}(\hat{\mathbf{r}}_i)\hat{\mathbf{q}}(\hat{\mathbf{r}}_i)\cdot\hat{\mathbf{v}}(\hat{\mathbf{r}}_i),$$

where $n_v = 4$ for the unit square and $n_v = 8$ for the unit cube. The transformation back to the physical element E yields

$$\left(K^{-1}\mathbf{q},\mathbf{v}\right)_{Q,E} = \frac{1}{n_v}\sum_{i=1}^{n_v} J_E(\hat{\mathbf{r}}_i)DF_E^{-T}(\mathbf{r}_i)DF_E^T(\hat{\mathbf{x}}_c)\overline{K}_E^{-1}\mathbf{q}(\mathbf{r}_i)\cdot\mathbf{v}(\mathbf{r}_i). \tag{12}$$

Given this local formula, the global quadrature rule is derived from (10). Note that the expression (12) induces a non-symmetric discrete bilinear form unless the Jacobian matrix DF_E is constant. In fact, if the mesh consists of parallelograms or parallelepipeds and the permeability is an element by element piecewise constant tensor, (12) becomes symmetric and reduces to (11).

2.6. The semidiscrete scheme

The MFMFE approximation to (3) on quadrilaterals and hexahedra reads: *Find* $(\mathbf{u}_h, p_h) : [0,T] \to V_h \times W_h$ *such that*

$$(p_{h,t}, w) + (\nabla\cdot\mathbf{u}_h, w) = (f, w) \qquad \forall w \in W_h, \tag{13a}$$

$$\left(K^{-1}\mathbf{u}_h,\mathbf{v}\right)_Q = (p_h, \nabla\cdot\mathbf{v}) - \left\langle g, \Pi_h^0\mathbf{v}\cdot\mathbf{n}\right\rangle_{\Gamma_D} \qquad \forall\mathbf{v}\in V_h, \tag{13b}$$

$$p_h(0) = \mathcal{S}_h p(0), \tag{13c}$$

where $\mathcal{S}_h p(0)$ denotes the elliptic MFE projection of p_0 (to be defined below). Note that the initial condition $p_h(0)$ determines $\mathbf{u}_h(0)$ through (13b). The use of Π_h^0 in (13b) permits to control the numerical quadrature error underlying the semidiscretization (cf. [5,6]). In this case, the discrete bilinear form $(K^{-1}\cdot,\cdot)_Q$ can be either symmetric, if given by (10) and (11), or non-symmetric, if given by (10) and (12). We call the resulting scheme a symmetric or non-symmetric MFMFE method depending on the choice of quadrature rule. As we shall see below, the introduction of a non-symmetric variant of the method is motivated by the loss of convergence that is observed when the symmetric scheme is applied to highly distorted quadrilateral and hexahedral meshes (cf. [7]).

In the case of simplicial elements, there is no need to project the non-homogeneous Dirichlet boundary data onto V_h^0. Further, due to the geometry of simplicial meshes, the use of a non-symmetric quadrature rule is not required. As a result, the MFMFE method is defined as above, with $(K^{-1}\cdot,\cdot)_Q$ given by (10) and (11), but removing the projection operator Π_h^0 from (13b).

2.7. Reduction to a cell-centered finite difference scheme for the pressure

In this subsection, we describe how the MFMFE formulation (13) reduces to a cell-centered finite difference scheme for the pressure. More precisely, we express the velocity degrees of freedom in terms of the pressure degrees of freedom via the quadrature rule in (13b), and substitute them back into (13a) in order to obtain a single equation for the pressure unknown.

To this end, let us first introduce the vector space $\mathcal{H}_v$ of semidiscrete velocity functions $U_h \equiv U_h(t) \in \mathbb{R}^L$, whose degrees of freedom are located at the vertices of each face (edge). We denote $L = nN_\ell$, where n is the number of vertices per face (edge) and N_ℓ denotes the number of faces (edges) in $\mathcal{T}_h$. A generic element of $\mathcal{H}_v$ has the form $U_h = (U_{h,1}, U_{h,2}, \ldots, U_{h,N_v})^T$, where $U_{h,i}\in\mathbb{R}^{\ell_i}$. In this case, ℓ_i is the number of faces (edges) that share the vertex point i and N_v denotes the number of vertices in $\mathcal{T}_h$. Note that the component of $U_{h,i}$ associated to the face (edge) e_j is given by the volumetric flux $(\mathbf{u}_h\cdot\mathbf{n}_{e_j})(\mathbf{r}_i)|e_j|$, where $|e_j|$ denotes the area (length) of e_j, for $j = 1,2,\ldots,\ell_i$. On the other hand, we

consider the vector space $\mathcal{H}_p$ of semidiscrete pressure functions $P_h \equiv P_h(t) \in \mathbb{R}^{N_e}$, whose degrees of freedom are located at the geometric centers of the cells. Here, N_e denotes the number of elements in $\mathcal{T}_h$. A generic element of $\mathcal{H}_p$ is considered to be $P_h = (P_{h,1}, P_{h,2}, \ldots, P_{h,N_e})^T$, where $P_{h,i} = p_h(\mathbf{x}_{c,i})$ and $\mathbf{x}_{c,i}$ denotes the coordinate vector of the cell center i.

Let $\{\mathbf{v}_i\}_{i=1}^{L}$ and $\{w_j\}_{j=1}^{N_e}$ be the bases of V_h and W_h, respectively. The differential system stemming from (13a)–(13b) is defined as

$$\begin{pmatrix} 0 \\ P_h' \end{pmatrix} + \begin{pmatrix} M & B^T \\ -D^{-1}B & 0 \end{pmatrix} \begin{pmatrix} U_h \\ P_h \end{pmatrix} = \begin{pmatrix} G_h \\ F_h \end{pmatrix} \tag{14}$$

where the matrices $M \in \mathbb{R}^{L\times L}$ and $B \in \mathbb{R}^{N_e\times L}$ are given by $(M)_{ij} = (K^{-1}\mathbf{v}_j, \mathbf{v}_i)_Q$ and $(B)_{ij} = -(\nabla\cdot\mathbf{v}_j, w_i)$, respectively. In addition, $D \in \mathbb{R}^{N_e\times N_e}$ is a diagonal matrix of the form $D = \mathrm{diag}(|E_1|, |E_2|, \ldots, |E_{N_e}|)$, where $|E_i|$ denotes the volume (area) of E_i, for $i = 1, 2, \ldots, N_e$. Finally, $G_h \in \mathbb{R}^L$ and $F_h \in \mathbb{R}^{N_e}$ contain the respective contributions of the Dirichlet boundary data g and the right-hand side f.

The choice of the trapezoidal quadrature rule $(K^{-1}\cdot,\cdot)_Q$ permits to decouple the velocity degrees of freedom associated to a vertex from the rest of them. In consequence, the assembled velocity mass matrix M has a block-diagonal structure,[1] i.e.,

$$M = \mathrm{diag}(M_1, M_2, \ldots, M_{N_v}), \tag{15}$$

where each block $M_i \in \mathbb{R}^{\ell_i\times\ell_i}$ is a local matrix associated to the vertex point i, for $i = 1, 2, \ldots, N_v$. The inversion of M in the first equation of (14) allows for the velocity function U_h to be expressed in terms of the pressure P_h, namely

$$U_h = M^{-1}\big(G_h - B^T P_h\big). \tag{16}$$

Since M is block-diagonal, this operation is locally performed on each block M_i. As a result, the velocity degrees of freedom associated to corner i are expressed in terms of the pressures located at the centers of the elements that share such a corner. Substituting (16) into the second equation of (14) leads to a cell-centered system for the pressures, i.e.,

$$P_h' + D^{-1}BM^{-1}B^T P_h = F_h + D^{-1}BM^{-1}G_h.$$

If we denote

$$A_h = D^{-1}BM^{-1}B^T, \qquad C_h = D^{-1}BM^{-1}G_h, \tag{17}$$

we can rewrite the MFMFE semidiscrete scheme (13) as a stiff initial value problem of the form: *Find* $P_h : [0, T] \to \mathcal{H}_p$ *such that*

$$P_h'(t) + A_h P_h(t) = F_h(t) + C_h(t), \quad t \in (0, T], \tag{18a}$$

$$P_h(0) = P_h^0, \tag{18b}$$

where F_h and P_h^0 are given element-wise by

$$\big(F_h(t)\big)_E = \frac{1}{|E|}\int_E f(\mathbf{x}, t)\,d\mathbf{x}, \qquad \big(P_h^0\big)_E = \frac{1}{|E|}\int_E p_0(\mathbf{x})\,d\mathbf{x},$$

respectively, for all $E \in \mathcal{T}_h$. The discrete diffusion operator A_h has a 27-point or 9-point stencil on logically cubic or rectangular grids, respectively.

2.8. Coercivity of the discrete bilinear form $(K^{-1}\cdot,\cdot)_Q$

The coercivity of the discrete bilinear forms induced by the quadrature rules introduced in Section 2.5 is a crucial requirement in the forthcoming analysis.

In the symmetric case, it is not difficult to verify that the quadrature rule given by (10) and (11) always induces a coercive discrete bilinear form in V_h, i.e.,

$$\big(K^{-1}\mathbf{q}, \mathbf{q}\big)_Q \geqslant \beta_0\|\mathbf{q}\|^2 \quad \forall\mathbf{q} \in V_h, \tag{19}$$

where β_0 is a positive constant, defined to be independent of h. The proof of (19) can be found in [1], for simplices and quadrilaterals, or [5], for hexahedra.

[1] Since M is induced by the discrete bilinear form $(K^{-1}\cdot,\cdot)_Q$, the symmetry of the corresponding blocks M_i will be determined by the local quadrature rule under consideration, i.e.: if $(K^{-1}\cdot,\cdot)_{Q,E}$ is given by (11), M_i will be symmetric; otherwise, if it is given by (12), M_i will be non-symmetric unless the mesh is composed of parallelogram or parallelepiped elements.

On the other hand, the coercivity of the non-symmetric discrete bilinear form induced by (10) and (12) is only guaranteed under certain restrictions on the element geometry and/or the anisotropy of tensor K. In order to derive such restrictions, we first rewrite the quadrature rule in the form

$$\left(K^{-1}\mathbf{q},\mathbf{v}\right)_Q = \sum_{E\in\mathcal{T}_h}\left(K^{-1}\mathbf{q},\mathbf{v}\right)_{Q,E} \equiv \sum_{i=1}^{N_v}\mathbf{v}_i^T M_i \mathbf{q}_i,$$

where $\mathbf{v}_i \equiv \{(\mathbf{v}\cdot\mathbf{n}_{e_j})(\mathbf{r}_i)|e_j|\}_{j=1}^{\ell_i}$ (with a similar definition for $\mathbf{q}_i$), $\mathbf{r}_i$ is the coordinate vector of the vertex point i and ℓ_i is the number of faces (edges) that share such a vertex. Moreover, $M_i \in \mathbb{R}^{\ell_i\times\ell_i}$ are the local matrices which form the global matrix M given by (15), for $i = 1, 2, \ldots, N_v$. Then, under the following condition,

$$\xi^T M_i \xi \geqslant C h^d \xi^T \xi \quad \forall \xi \in \mathbb{R}^{\ell_i}, \tag{20}$$

$(K^{-1}\cdot,\cdot)_Q$ is coercive in V_h and satisfies (19). If, in addition,

$$\xi^T M_i^T M_i \xi \leqslant C h^{2d} \xi^T \xi \quad \forall \xi \in \mathbb{R}^{\ell_i}, \tag{21}$$

the discrete bilinear form is also continuous in V_h, i.e.,

$$\left(K^{-1}\mathbf{q},\mathbf{v}\right)_Q \leqslant \beta_1 \|\mathbf{q}\|\|\mathbf{v}\| \quad \forall \mathbf{q},\mathbf{v}\in V_h, \tag{22}$$

where β_1 is a positive constant, defined to be independent of h (cf. [7]). Further details on the conditions (20) and (21) are discussed in [3,35].

3. The elliptic mixed finite element projection

The error analysis of the semidiscrete scheme (13) requires the introduction of a so-called elliptic MFE projection operator. Such an operator was first suggested in [36] and has been subsequently used in, e.g., [37,38]. In particular, the variational formulation (3) admits an elliptic MFE projection of the form: *Find* $(\mathcal{R}_h\mathbf{u}, \mathcal{S}_h p) : [0, T] \to V_h \times W_h$ *such that*

$$(\nabla\cdot\mathcal{R}_h\mathbf{u}, w) = (f - p_t, w) \qquad \forall w \in W_h, \tag{23a}$$

$$\left(K^{-1}\mathcal{R}_h\mathbf{u},\mathbf{v}\right)_Q = (\mathcal{S}_h p, \nabla\cdot\mathbf{v}) - \left\langle g, \Pi_h^0\mathbf{v}\cdot\mathbf{n}\right\rangle_{\Gamma_D} \qquad \forall \mathbf{v}\in V_h, \tag{23b}$$

$$\left(\mathcal{S}_h p(0), w\right) = (p_0, w) \qquad \forall w \in W_h. \tag{23c}$$

Note that the pair $(\mathcal{R}_h\mathbf{u}, \mathcal{S}_h p)$ is precisely the solution of the MFE approximation to a continuous elliptic problem whose exact solution is $(\mathbf{u}, p)$. Subtracting (23) from (3), we get the error equations

$$\begin{aligned}
&\left(\nabla\cdot(\mathbf{u}-\mathcal{R}_h\mathbf{u}), w\right) = 0 && \forall w\in W_h,\\
&\left(K^{-1}\mathbf{u},\mathbf{v}\right) - \left(K^{-1}\mathcal{R}_h\mathbf{u},\mathbf{v}\right)_Q = (p-\mathcal{S}_h p, \nabla\cdot\mathbf{v}) - \left\langle g, \left(\mathbf{v}-\Pi_h^0\mathbf{v}\right)\cdot\mathbf{n}\right\rangle_{\Gamma_D} && \forall \mathbf{v}\in V_h,\\
&\left(p(0)-\mathcal{S}_h p(0), w\right) = 0 && \forall w\in W_h.
\end{aligned}$$

The local quadrature error on each element is defined to be

$$\sigma_E(\mathbf{q},\mathbf{v}) \equiv (\mathbf{q},\mathbf{v})_E - (\mathbf{q},\mathbf{v})_{Q,E},$$

in such a way that $\sigma(\mathbf{q},\mathbf{v})|_E \equiv \sigma_E(\mathbf{q},\mathbf{v})$ represents the global quadrature error. Taking into account (8), the previous equations can be rewritten as

$$\left(\nabla\cdot(\mathbf{u}-\mathcal{R}_h\mathbf{u}), w\right) = 0 \qquad \forall w\in W_h, \tag{24a}$$

$$\left(K^{-1}(\mathbf{u}-\mathcal{R}_h\mathbf{u}),\mathbf{v}\right) + \sigma\left(K^{-1}\mathcal{R}_h\mathbf{u},\mathbf{v}\right) = (\mathcal{P}_h p - \mathcal{S}_h p, \nabla\cdot\mathbf{v}) - \left\langle g, \left(\mathbf{v}-\Pi_h^0\mathbf{v}\right)\cdot\mathbf{n}\right\rangle_{\Gamma_D} \qquad \forall \mathbf{v}\in V_h. \tag{24b}$$

Let us now recall some convergence results derived for the elliptic case in two- and three-dimensional meshes. The results related to the symmetric MFMFE method assume certain restrictions on the element geometry (in the case of quadrilaterals and hexahedra), which are described in the sequel. Following the terminology from [1,5,6], we call *generalized quadrilaterals* the (possibly non-planar) faces of a hexahedral element E defined via a trilinear mapping F_E of the form (5). A generalized quadrilateral with vertices $\mathbf{r}_1$, $\mathbf{r}_2$, $\mathbf{r}_3$ and $\mathbf{r}_4$ is called an h^2*-parallelogram* if

$$|\mathbf{r}_{34} - \mathbf{r}_{21}|_{\mathbb{R}^d} \leqslant C h^2.$$

Elements of this kind are obtained by uniform refinements of a general quadrilateral grid. Furthermore, a hexahedral element is called an h^2*-parallelepiped* if all of its faces are h^2-parallelograms. Recalling (5), this condition implies that $\partial_{\hat{x}\hat{y}}F_E$, $\partial_{\hat{x}\hat{z}}F_E$ and $\partial_{\hat{y}\hat{z}}F_E$ are $\mathcal{O}(h^2)$. Finally, an h^2-parallelepiped is called *regular* if

$$\left|(\mathbf{r}_{21}-\mathbf{r}_{34})-(\mathbf{r}_{65}-\mathbf{r}_{78})\right|_{\mathbb{R}^d}\leqslant Ch^3.$$

This condition implies that $\partial_{\hat{x}\hat{y}\hat{z}}F_E$ is $\mathcal{O}(h^3)$.

In the following subsections, $W^{\alpha,\infty}_{\mathcal{T}_h}$ denotes a space consisting of functions φ such that $\varphi|_E\in W^{\alpha,\infty}(E)$ for all $E\in\mathcal{T}_h$, α being an integer.

3.1. Optimal convergence for the velocity

On simplicial grids or h^2-perturbed quadrilateral and hexahedral grids, the symmetric MFMFE elliptic projection gives first-order convergence for the velocity.

Lemma 1. *(See Wheeler–Yotov [1, Theorem 3.4], Ingram–Wheeler–Yotov [5, Theorem 3.1].) If $K^{-1}\in W^{1,\infty}_{\mathcal{T}_h}$, then the velocity $\mathcal{R}_h\mathbf{u}(t)$ of the symmetric MFMFE elliptic projection (23), with the quadrature rule (10) and (11), satisfies, for all $t\in[0,T]$,*

$$\left\|\mathbf{u}(t)-\mathcal{R}_h\mathbf{u}(t)\right\|\leqslant Ch\|\mathbf{u}\|_1 \tag{25}$$

on simplices, h^2-parallelograms and h^2-parallelepipeds, where C is a positive constant, defined to be independent of h.

On distorted quadrilateral and hexahedral grids, the non-symmetric MFMFE elliptic projection also gives first-order convergence for the velocity.

Lemma 2. *(See Wheeler–Xue–Yotov [7, Theorem 3.1].) Let $K\in W^{1,\infty}_{\mathcal{T}_h}$ and $K^{-1}\in W^{0,\infty}_{\mathcal{T}_h}$. If (20) and (21) hold, then the velocity $\mathcal{R}_h\mathbf{u}(t)$ of the non-symmetric MFMFE elliptic projection (23), with the quadrature rule (10) and (12), satisfies, for all $t\in[0,T]$,*

$$\left\|\Pi_h\mathbf{u}(t)-\mathcal{R}_h\mathbf{u}(t)\right\|\leqslant Ch\big(|\mathbf{u}|_1+\|p\|_2\big) \tag{26}$$

on general quadrilaterals and hexahedra, where C is a positive constant, defined to be independent of h.

Based on the previous lemma, we can also derive a convergence result for the velocity on the element faces (edges). To this end, we introduce a norm for vectors in Ω which considers the normal components on the faces (edges) of $\mathcal{T}_h$, i.e.,

$$\|\mathbf{v}\|^2_{\mathcal{F}_h}=\sum_{E\in\mathcal{T}_h}\sum_{e\in\partial E}\frac{|E|}{|e|}\|\mathbf{v}\cdot\mathbf{n}_e\|^2_e, \tag{27}$$

where $|E|$ is the volume (area) of E and $|e|$ is the area (length) of e.

Lemma 3. *(See Wheeler–Xue–Yotov [7, Theorem 3.2].) Let $K\in W^{1,\infty}_{\mathcal{T}_h}$ and $K^{-1}\in W^{0,\infty}_{\mathcal{T}_h}$. If (20) and (21) hold, then the velocity $\mathcal{R}_h\mathbf{u}(t)$ of the non-symmetric MFMFE elliptic projection (23), with the quadrature rule (10) and (12), satisfies, for all $t\in[0,T]$,*

$$\left\|\mathbf{u}(t)-\mathcal{R}_h\mathbf{u}(t)\right\|_{\mathcal{F}_h}\leqslant Ch\big(\|\mathbf{u}\|_1+\|p\|_2\big) \tag{28}$$

on general quadrilaterals and hexahedra, where C is a positive constant, defined to be independent of h.

Note that the results of the last two lemmas were obtained in [7] for the case of homogeneous Dirichlet boundary conditions. The extension of such results to the case under study, involving non-homogeneous Dirichlet and homogeneous Neumann boundary data, is straightforward. Further details are omitted.

3.2. Optimal convergence for the pressure

Under the assumptions of the preceding lemmas, the pressure variable is observed to be first-order convergent in both the symmetric and the non-symmetric MFMFE elliptic projections.

Lemma 4. *(See Wheeler–Yotov [1, Theorem 4.1], Ingram–Wheeler–Yotov [5, Theorem 4.1].) If $K^{-1}\in W^{1,\infty}_{\mathcal{T}_h}$, then the pressure $\mathcal{S}_hp(t)$ of the symmetric MFMFE elliptic projection (23), with the quadrature rule (10) and (11), satisfies, for all $t\in[0,T]$,*

$$\left\|p(t)-\mathcal{S}_hp(t)\right\|\leqslant Ch\big(\|\mathbf{u}\|_1+\|p\|_1\big) \tag{29}$$

on simplices, h^2-parallelograms and h^2-parallelepipeds, where C is a positive constant, defined to be independent of h.

Lemma 5. *(See Wheeler–Xue–Yotov [7, Theorem 4.1].) Let $K \in W^{1,\infty}_{\mathcal{T}_h}$ and $K^{-1} \in W^{0,\infty}_{\mathcal{T}_h}$. If (20) and (21) hold, then the pressure $\mathcal{S}_h p(t)$ of the non-symmetric MFMFE elliptic projection (23), with the quadrature rule (10) and (12), satisfies, for all $t \in [0, T]$,*

$$\left\| p(t) - \mathcal{S}_h p(t) \right\| \leqslant Ch\left(|\mathbf{u}|_1 + \|p\|_2 \right) \tag{30}$$

on general quadrilaterals and hexahedra, where C is a positive constant, defined to be independent of h.

As mentioned above, the subsequent analysis considers an extension of the result of Lemma 5, derived in [7] for a problem with homogeneous Dirichlet boundary data, to the case of dealing with boundary conditions of the form (1c) and (1d).

3.3. Superconvergence for the pressure

In addition, the symmetric MFMFE elliptic projection shows second-order superconvergence for the pressure variable at the center of mass of the elements.

Lemma 6. *(See Wheeler–Yotov [1, Theorem 4.3], Ingram–Wheeler–Yotov [5, Theorem 4.2].) Let $K \in W^{1,\infty}_{\mathcal{T}_h}$ and $K^{-1} \in W^{2,\infty}_{\mathcal{T}_h}$. If H^2-elliptic regularity holds, then the pressure $\mathcal{S}_h p(t)$ of the symmetric MFMFE elliptic projection (23), with the quadrature rule (10) and (11), satisfies, for all $t \in [0, T]$,*

$$\left\| \mathcal{P}_h p(t) - \mathcal{S}_h p(t) \right\| \leqslant Ch^2\left(\|\mathbf{u}\|_1 + \|\nabla \cdot \mathbf{u}\|_1 \right) \tag{31}$$

on simplices and

$$\left\| \mathcal{P}_h p(t) - \mathcal{S}_h p(t) \right\| \leqslant Ch^2 \|\mathbf{u}\|_2 \tag{32}$$

on h^2-parallelograms and regular h^2-parallelepipeds, where C is a positive constant, defined to be independent of h.

4. Error analysis of the semidiscrete scheme

In order to derive a priori error estimates for the MFMFE semidiscrete formulation (13), we need to bound the distance between the elliptic projection $(\mathcal{R}_h \mathbf{u}, \mathcal{S}_h p)$ and the semidiscrete solution $(\mathbf{u}_h, p_h)$. The subsequent combination of such bounds and the corresponding results from the previous lemmas yields the convergence for both the velocity and the pressure variables.

4.1. Optimal convergence for the velocity

The symmetric variant of the MFMFE method shows optimal convergence of order $\mathcal{O}(h)$ for the velocity variable in the time–space norm $L^\infty(L^2)$.

Theorem 1. *Under the hypotheses of Lemma 1, the velocity $\mathbf{u}_h(t)$ of the symmetric MFMFE method (13), with the quadrature rule (10) and (11), satisfies*

$$\|\mathbf{u} - \mathbf{u}_h\|_{L^\infty(L^2)} \leqslant Ch\left(\|\mathbf{u}\|_{L^\infty(H^1)} + \|\mathbf{u}\|_{L^2(H^1)} + \|p_t\|_{L^2(H^1)} \right) \tag{33}$$

on simplices, h^2-parallelograms and h^2-parallelepipeds, where C is a positive constant, defined to be independent of h.

Proof. For all $t \in [0, T]$, let us split the error term in the $L^2(\Omega)$-norm by using the triangle inequality, i.e.,

$$\|\mathbf{u} - \mathbf{u}_h\| \leqslant \|\mathbf{u} - \mathcal{R}_h \mathbf{u}\| + \|\mathcal{R}_h \mathbf{u} - \mathbf{u}_h\|. \tag{34}$$

Subtracting (13) from (3), we get the error equations

$$\begin{aligned}
&(p_t - p_{h,t}, w) + \left(\nabla \cdot (\mathbf{u} - \mathbf{u}_h), w\right) = 0 && \forall w \in W_h,\\
&\left(K^{-1}\mathbf{u}, \mathbf{v}\right) - \left(K^{-1}\mathbf{u}_h, \mathbf{v}\right)_Q = (p - p_h, \nabla \cdot \mathbf{v}) - \left\langle g, \left(\mathbf{v} - \Pi_h^0 \mathbf{v}\right) \cdot \mathbf{n} \right\rangle_{\Gamma_D} && \forall \mathbf{v} \in V_h,\\
&\left(p(0) - p_h(0), w\right) = 0 && \forall w \in W_h.
\end{aligned}$$

Let us shorten the notations by setting

$$\xi_h = \mathcal{S}_h p - p_h, \qquad \gamma_h = p - \mathcal{S}_h p, \qquad \zeta_h = \mathcal{R}_h \mathbf{u} - \mathbf{u}_h. \tag{35}$$

Then, taking into account (24), we get

$$(\xi_{h,t} + \gamma_{h,t}, w) + (\nabla \cdot \zeta_h, w) = 0 \quad \forall w \in W_h, \tag{36a}$$

$$\left(K^{-1}\zeta_h, \mathbf{v}\right)_Q = (\xi_h, \nabla \cdot \mathbf{v}) \quad \forall \mathbf{v} \in V_h, \tag{36b}$$

$$\xi_h(0) = 0. \tag{36c}$$

In this derivation, we use the easily established fact that the projection operator $\mathcal{S}_h$ commutes with time differentiation. If we further differentiate (36b) with respect to t, and choose $\mathbf{v} = \zeta_h$ and $w = \xi_{h,t}$, we get

$$(\xi_{h,t}, \xi_{h,t}) + \left(K^{-1}\zeta_{h,t}, \zeta_h\right)_Q = -(\gamma_{h,t}, \xi_{h,t}), \tag{37}$$

by adding the resulting equations. Since the discrete bilinear form $(K^{-1}\cdot, \cdot)_Q$ is symmetric, it satisfies

$$\left(K^{-1}\zeta_{h,t}, \zeta_h\right)_Q = \frac{1}{2}\frac{d}{dt}\left(K^{-1}\zeta_h, \zeta_h\right)_Q. \tag{38}$$

Thus, (37) can be expressed as

$$\|\xi_{h,t}\|^2 + \frac{1}{2}\frac{d}{dt}\left(K^{-1}\zeta_h, \zeta_h\right)_Q \leqslant \frac{1}{2}\left(\|\gamma_{h,t}\|^2 + \|\xi_{h,t}\|^2\right), \tag{39}$$

where we use the Cauchy–Schwarz inequality and Young's inequality in the form

$$ab \leqslant \frac{1}{2}\left(\epsilon a^2 + \frac{1}{\epsilon}b^2\right) \quad \forall a, b \geqslant 0,$$

with $\epsilon = 1$. Note that the first term in (39) is non-negative. Integrating this expression with respect to t and taking into account the coercivity (19) of $(K^{-1}\cdot, \cdot)_Q$, we obtain

$$\left\|\zeta_h(t)\right\|^2 \leqslant \frac{1}{\beta_0}\int_0^t \|\gamma_{h,t}\|^2 \, d\tau,$$

for all $t \in [0, T]$. Since $\xi_h(0) = 0$, then $\zeta_h(0) = 0$, as can be derived from (36b) by taking $\mathbf{v} = \zeta_h(0)$. The right-hand side of the previous inequality is bounded by (29). This result, together with (25) and (34), yields

$$\left\|\mathbf{u}(t) - \mathbf{u}_h(t)\right\|^2 \leqslant Ch^2\left(\left\|\mathbf{u}(t)\right\|_1^2 + \int_0^t \left(\|\mathbf{u}\|_1^2 + \|p_t\|_1^2\right) d\tau\right),$$

for all $t \in [0, T]$. Taking the supremum over all t, we obtain (33) and complete the proof. □

In the non-symmetric case, the argument in Theorem 1 does not apply. The next theorem proves convergence of the semidiscrete velocity $\mathbf{u}_h(t)$ to the MFE projection of the true solution $\Pi_h\mathbf{u}(t)$ with order $\mathcal{O}(h)$ in the time–space norm $L^2(L^2)$.

Theorem 2. *Under the hypotheses of Lemma 2, the velocity $\mathbf{u}_h(t)$ of the non-symmetric MFMFE method (13), with the quadrature rule (10) and (12), satisfies*

$$\|\Pi_h\mathbf{u} - \mathbf{u}_h\|_{L^2(L^2)} \leqslant Ch\left(\|\mathbf{u}\|_{L^2(H^1)} + \|p\|_{L^2(H^2)} + \|p_t\|_{L^2(H^2)}\right) \tag{40}$$

on general quadrilaterals and hexahedra, where C is a positive constant, defined to be independent of h.

Proof. In this case, for all $t \in [0, T]$, the error term in the $L^2(\Omega)$-norm is split into

$$\|\Pi_h\mathbf{u} - \mathbf{u}_h\| \leqslant \|\Pi_h\mathbf{u} - \mathcal{R}_h\mathbf{u}\| + \|\mathcal{R}_h\mathbf{u} - \mathbf{u}_h\|. \tag{41}$$

Let us consider the error equations (36). Since the pair (ζ_h, ξ_h) belongs to $V_h \times W_h$, we may choose $\mathbf{v} = \zeta_h$ and $w = \xi_h$. Then, by adding (36a) and (36b), we obtain

$$(\xi_{h,t}, \xi_h) + \left(K^{-1}\zeta_h, \zeta_h\right)_Q = -(\gamma_{h,t}, \xi_h).$$

Now, we bound the terms on the left-hand side from below and bound those on the right-hand side from above. Using the coercivity (19) of $(K^{-1}\cdot, \cdot)_Q$, together with the Cauchy–Schwarz and Young's inequalities, we get

$$\frac{1}{2}\frac{d}{dt}\|\xi_h\|^2 + \beta_0\|\zeta_h\|^2 \leqslant \frac{1}{2}\left(\|\gamma_{h,t}\|^2 + \|\xi_h\|^2\right).$$

Integrating with respect to the time variable from 0 to t, we obtain

$$\left\|\xi_h(t)\right\|^2 + 2\beta_0 \int_0^t \|\zeta_h\|^2 \, d\tau \leqslant \int_0^t \left(\|\gamma_{h,t}\|^2 + \|\xi_h\|^2\right) d\tau,$$

for all $t \in [0, T]$, using that $\xi_h(0) = 0$. The subsequent application of Gronwall's lemma yields

$$\left\|\xi_h(t)\right\|^2 + 2\beta_0 \int_0^t \|\zeta_h\|^2 \, d\tau \leqslant C \int_0^t \|\gamma_{h,t}\|^2 \, d\tau, \tag{42}$$

for all $t \in [0, T]$. At $t = T$, it holds

$$\int_0^T \|\zeta_h\|^2 \, d\tau \leqslant \frac{C}{2\beta_0} \int_0^T \|\gamma_{h,t}\|^2 \, d\tau.$$

Thus, (40) follows by recalling (30) for the right-hand side, together with (26) and (41). □

In addition, first-order convergence is also observed for the velocity of the non-symmetric method on the element faces (edges). The following result is given in the norm

$$\|\mathbf{v}\|_{L^2([0,T];\mathcal{F}_h)} \equiv \|\mathbf{v}\|_{L^2(\mathcal{F}_h)} = \left(\int_0^T \left\|\mathbf{v}(t)\right\|_{\mathcal{F}_h}^2 dt \right)^{1/2},$$

where $\|\cdot\|_{\mathcal{F}_h}$ is defined in (27).

Theorem 3. *Under the hypotheses of Lemma 3, the velocity $\mathbf{u}_h(t)$ of the non-symmetric MFMFE method (13), with the quadrature rule (10) and (12), satisfies*

$$\|\mathbf{u} - \mathbf{u}_h\|_{L^2(\mathcal{F}_h)} \leqslant Ch\left(\|\mathbf{u}\|_{L^2(H^1)} + \|p\|_{L^2(H^2)} + \|p_t\|_{L^2(H^2)}\right) \tag{43}$$

on general quadrilaterals and hexahedra, where C is a positive constant, defined to be independent of h.

Proof. For all $t \in [0, T]$, the error term in the norm $\|\cdot\|_{\mathcal{F}_h}$ is split into

$$\|\mathbf{u} - \mathbf{u}_h\|_{\mathcal{F}_h} \leqslant \|\mathbf{u} - \mathcal{R}_h\mathbf{u}\|_{\mathcal{F}_h} + \|\mathcal{R}_h\mathbf{u} - \mathbf{u}_h\|_{\mathcal{F}_h}. \tag{44}$$

In order to obtain a suitable bound for the second term on the right-hand side, we first note that

$$\|\mathcal{R}_h\mathbf{u} - \mathbf{u}_h\|_{\mathcal{F}_h} \leqslant C\|\mathcal{R}_h\mathbf{u} - \mathbf{u}_h\|. \tag{45}$$

This follows from the trace inequality (cf. [7, Lemma 3.9])

$$\|\mathbf{v} \cdot \mathbf{n}_e\|_e \leqslant Ch^{-1/2}\|\mathbf{v}\|_E \quad \forall \mathbf{v} \in V_h,$$

and the shape regularity of $\mathcal{T}_h$, which implies

$$\|\mathbf{v}\|_{\mathcal{F}_h} \leqslant Ch^{1/2}\left(\sum_{E \in \mathcal{T}_h} \sum_{e \in \partial E} \|\mathbf{v} \cdot \mathbf{n}_e\|_e^2 \right)^{1/2},$$

by using $|E|/|e| = \mathcal{O}(h)$. Then, along the lines of the preceding theorem, (43) follows from (28), (30), (44) and (45). □

4.2. Optimal convergence for the pressure

Both the symmetric and the non-symmetric MFMFE methods show first-order convergence for the pressure variable in the time–space norm $L^\infty(L^2)$. The corresponding error estimates are derived in the sequel.

Theorem 4. *Under the hypotheses of Lemma 4, the pressure $p_h(t)$ of the symmetric MFMFE method (13), with the quadrature rule (10) and (11), satisfies*

$$\|p - p_h\|_{L^\infty(L^2)} \leqslant Ch\left(\|\mathbf{u}\|_{L^\infty(H^1)} + \|\mathbf{u}\|_{L^2(H^1)} + \|p\|_{L^\infty(H^1)} + \|p_t\|_{L^2(H^1)}\right) \tag{46}$$

on simplices, h^2-parallelograms and h^2-parallelepipeds, where C is a positive constant, defined to be independent of h.

Proof. For all $t \in [0, T]$, let us split the error term in the $L^2(\Omega)$-norm by using the triangle inequality, i.e.,

$$\|p - p_h\| \leqslant \|p - \mathcal{S}_h p\| + \|\mathcal{S}_h p - p_h\|. \tag{47}$$

Following the argument of Theorem 2, we may derive the inequality (42). Since the second term in this expression is non-negative, we have

$$\left\|\xi_h(t)\right\|^2 \leqslant C \int_0^t \|\gamma_{h,t}\|^2 \, d\tau,$$

for all $t \in [0, T]$. Inserting this bound into (47) and using (29) to control its right-hand side, we obtain

$$\left\|p(t) - p_h(t)\right\|^2 \leqslant Ch^2 \left(\left\|\mathbf{u}(t)\right\|_1^2 + \left\|p(t)\right\|_1^2 + \int_0^t \left(\|\mathbf{u}\|_1^2 + \|p_t\|_1^2 \right) d\tau \right),$$

for all $t \in [0, T]$. The proof is completed by taking the supremum over all t. □

Theorem 5. *Under the hypotheses of Lemma 5, the pressure $p_h(t)$ of the non-symmetric MFMFE method (13), with the quadrature rule (10) and (12), satisfies*

$$\|p - p_h\|_{L^\infty(L^2)} \leqslant Ch\left(\|\mathbf{u}\|_{L^\infty(H^1)} + \|\mathbf{u}\|_{L^2(H^1)} + \|p\|_{L^\infty(H^2)} + \|p_t\|_{L^2(H^2)} \right) \tag{48}$$

on general quadrilaterals and hexahedra, where C is a positive constant, defined to be independent of h.

Proof. The proof is analogous to that of the previous theorem. In this case, we make use of the expression (30), related to the non-symmetric method, for bounding the term $\|p - \mathcal{S}_h p\|$ and its time derivative. □

4.3. Superconvergence for the pressure

In the case of the symmetric MFMFE method, a superconvergence phenomenon of order $\mathcal{O}(h^2)$ is observed for the pressure variable at the center of mass of the elements.

Theorem 6. *Under the hypotheses of Lemma 6, the pressure $p_h(t)$ of the symmetric MFMFE method (13), with the quadrature rule (10) and (11), satisfies*

$$\|\mathcal{P}_h p - p_h\|_{L^\infty(L^2)} \leqslant Ch^2\left(\|\mathbf{u}\|_{L^\infty(H^1)} + \|\mathbf{u}\|_{L^2(H^1)} + \|\nabla \cdot \mathbf{u}\|_{L^\infty(H^1)} + \|\nabla \cdot \mathbf{u}\|_{L^2(H^1)} \right) \tag{49}$$

on simplices and

$$\|\mathcal{P}_h p - p_h\|_{L^\infty(L^2)} \leqslant Ch^2\left(\|\mathbf{u}\|_{L^\infty(H^2)} + \|\mathbf{u}\|_{L^2(H^2)} \right) \tag{50}$$

on h^2-parallelograms and regular h^2-parallelepipeds, where C is a positive constant, defined to be independent of h.

Proof. The proof is similar to that of Theorem 4. In this case, for all $t \in [0, T]$, the error term in the $L^2(\Omega)$-norm is split into

$$\|\mathcal{P}_h p - p_h\| \leqslant \|\mathcal{P}_h p - \mathcal{S}_h p\| + \|\mathcal{S}_h p - p_h\|.$$

In addition, we must redefine γ_h in (35) as $\gamma_h = \mathcal{P}_h p - \mathcal{S}_h p$. Then, using (31) and (32) to bound those terms involving γ_h and $\gamma_{h,t}$, we get (49) and (50), respectively, and complete the proof. □

5. The domain decomposition splitting method

Once the cell-centered finite difference method (18) is defined, we are in position to construct a suitable time integrator to approximate the semidiscrete solution. In this section, we first introduce an adequate operator splitting for the discrete diffusion and right-hand side, which belongs to the class of domain decomposition methods. Then, such a splitting is combined with a fractional step formula in order to reduce the system of ordinary differential equations (18) to a collection of algebraic linear systems (one per internal stage).

5.1. A domain decomposition operator splitting

In order to define the domain decomposition splitting technique, Ω is first partitioned into a number m of overlapping subdomains $\{\Omega_k\}_{k=1}^m$. Under such a decomposition, we subsequently introduce a family of m smooth functions $\{\rho_k(\mathbf{x})\}_{k=1}^m$ forming a partition of unity. Via this partition, both A_h and $F_h(t)$ are decomposed into m split terms to further apply a fractional step time integrator. The overall procedure is described in the sequel.

Let $\Omega_1^*, \Omega_2^*, \ldots, \Omega_m^*$ form a non-overlapping decomposition of Ω into m subdomains. Such a decomposition fulfills the conditions $\overline{\Omega} = \bigcup_{k=1}^m \overline{\Omega}_k^*$ and $\Omega_k^* \cap \Omega_l^* = \emptyset$, for $k \neq l$. In turn, each $\Omega_k^* \subset \Omega$ is considered to be an open disconnected set involving m_k connected components, i.e.,

$$\Omega_k^* \equiv \bigcup_{l=1}^{m_k} \Omega_{kl}^*, \quad \text{for } k = 1, 2, \ldots, m.$$

Such components are pairwise disjoint (that is, $\Omega_{ki}^* \cap \Omega_{kj}^* = \emptyset$, for $i \neq j$) and typically chosen to be shape regular of diameter h_0. For instance, the components Ω_{kl}^* may correspond to the elements in a coarse partition $\mathcal{T}_{h_0}$ of Ω with mesh size h_0.

Let Ω_{kl} be the extension of Ω_{kl}^* obtained by translating its internal boundaries, $\partial\Omega_{kl}^* \cap \Omega$, within a distance βh_0 in Ω. The parameter $\beta > 0$ is usually referred to as the overlapping factor and its value must be chosen in such a way that the extended components are also pairwise disjoint (i.e., $\Omega_{ki} \cap \Omega_{kj} = \emptyset$, for $i \neq j$). Furthermore, the distance $\xi = 2\beta h_0$ is called the overlapping size. If we denote by $\Omega_k \subset \Omega$ the open disconnected set defined as

$$\Omega_k \equiv \bigcup_{l=1}^{m_k} \Omega_{kl}, \quad \text{for } k = 1, 2, \ldots, m, \tag{51}$$

then the collection $\Omega_1, \Omega_2, \ldots, \Omega_m$ form an overlapping decomposition of Ω into m subdomains. Such a decomposition satisfies $\Omega = \bigcup_{k=1}^m \Omega_k$.

Subordinate to this overlapping covering of Ω, we construct a smooth partition of unity consisting of a family of m non-negative and $\mathcal{C}^\infty(\Omega)$ functions $\{\rho_k(\mathbf{x})\}_{k=1}^m$. Each function $\rho_k : \overline{\Omega} \to [0, 1]$ is chosen to be

$$\rho_k(\mathbf{x}) = \begin{cases} 0, & \text{if } \mathbf{x} \in \overline{\Omega} \setminus \overline{\Omega}_k, \\ h_k(\mathbf{x}), & \text{if } \mathbf{x} \in \bigcup_{l=1;\, l\neq k}^m (\overline{\Omega}_k \cap \overline{\Omega}_l), \\ 1, & \text{if } \mathbf{x} \in \overline{\Omega}_k \setminus \bigcup_{l=1;\, l\neq k}^m (\overline{\Omega}_k \cap \overline{\Omega}_l), \end{cases}$$

where $h_k(\mathbf{x})$ is $\mathcal{C}^\infty(\Omega)$ and satisfies the conditions

$$0 \leqslant h_k(\mathbf{x}) \leqslant 1, \quad \sum_{k=1}^m h_k(\mathbf{x}) = 1,$$

for any $\mathbf{x} \in \bigcup_{l=1;\, l\neq k}^m (\overline{\Omega}_k \cap \overline{\Omega}_l)$. Therefore, the family of functions $\{\rho_k(\mathbf{x})\}_{k=1}^m$ is such that

$$\operatorname{supp}\big(\rho_k(\mathbf{x})\big) \subset \overline{\Omega}_k, \qquad 0 \leqslant \rho_k(\mathbf{x}) \leqslant 1, \qquad \sum_{k=1}^m \rho_k(\mathbf{x}) = 1, \tag{52}$$

for any $\mathbf{x} \in \overline{\Omega}$. For numerical purposes, functions $h_k(\mathbf{x})$ which are not necessarily $\mathcal{C}^\infty(\Omega)$, but are continuous and piecewise smooth, can also be considered (cf. [19]). This fact will be illustrated in the last section of the paper.

In this framework, we introduce a splitting for the time derivative of the differential system (18a) based on the preceding partition of unity. In doing so, we first define two families of matrices, $\{\Gamma_k\}_{k=1}^m$ and $\{\tilde{\Gamma}_k\}_{k=1}^m$, associated to the overlapping decomposition $\{\Omega_k\}_{k=1}^m$. The first of such families is constructed in the spirit of the block-diagonal matrix M induced by $(K^{-1}\cdot, \cdot)_Q$ (see (15)). More precisely, each matrix $\Gamma_k \in \mathbb{R}^{L\times L}$ has a block-diagonal structure of the form

$$\Gamma_k = \begin{pmatrix} \rho_k(\mathbf{r}_1) I_{\ell_1} & & & \\ & \rho_k(\mathbf{r}_2) I_{\ell_2} & & \\ & & \ddots & \\ & & & \rho_k(\mathbf{r}_{N_v}) I_{\ell_{N_v}} \end{pmatrix}, \tag{53}$$

where $I_{\ell_i} \in \mathbb{R}^{\ell_i \times \ell_i}$ is the identity matrix and $\mathbf{r}_i$ denotes the coordinate vector of the vertex point i, for $i = 1, 2, \ldots, N_v$ and $k = 1, 2, \ldots, m$ (see Section 2.7 for notations). As for the second family of matrices, we consider $\tilde{\Gamma}_k \in \mathbb{R}^{N_e \times N_e}$ to be a diagonal matrix of the form

$$\tilde{\Gamma}_k = \begin{pmatrix} \rho_k(\mathbf{x}_{c,1}) & & & \\ & \rho_k(\mathbf{x}_{c,2}) & & \\ & & \ddots & \\ & & & \rho_k(\mathbf{x}_{c,N_e}) \end{pmatrix}, \tag{54}$$

where $\mathbf{x}_{c,i}$ denotes the coordinate vector of the cell center i, for $i = 1, 2, \ldots, N_e$ and $k = 1, 2, \ldots, m$. Note that, by construction,

$$\sum_{k=1}^{m} \Gamma_k = I_L, \qquad \sum_{k=1}^{m} \tilde{\Gamma}_k = I_{N_e}. \tag{55}$$

In this context, the explicit formula for the time derivative P_h', as given by the second equation in (14), is

$$P_h' = D^{-1} B U_h + F_h \equiv Q_h.$$

The time integration method described in the next subsection takes advantage of a suitable representation of Q_h as a sum of somewhat simpler terms, i.e.,

$$Q_h = Q_{h,1} + Q_{h,2} + \cdots + Q_{h,m},$$

where each split term is given by the expression

$$Q_{h,k} = D^{-1} B U_{h,k} + F_{h,k}, \tag{56}$$

for $k = 1, 2, \ldots, m$. More precisely, using the matrices (53) and (54), we define $U_{h,k} = \Gamma_k U_h$ and $F_{h,k} = \tilde{\Gamma}_k F_h$. Recall that the velocity degrees of freedom in U_h are located at the vertex points, while the semidiscrete right-hand side F_h lies on the cell centers. This is the reason why the partition of unity functions $\{\rho_k(\mathbf{x})\}_{k=1}^m$ are evaluated at different points in Γ_k and $\tilde{\Gamma}_k$. Due to (55), we have

$$U_h = \sum_{k=1}^{m} U_{h,k}, \qquad F_h = \sum_{k=1}^{m} F_{h,k}. \tag{57}$$

Using the expression (16) for U_h, the split velocity is given by

$$U_{h,k} = \Gamma_k M^{-1} \left(G_h - B^T P_h \right),$$

and can be inserted into (56) to get

$$Q_{h,k} = D^{-1} B \Gamma_k M^{-1} \left(G_h - B^T P_h \right) + F_{h,k}.$$

Based on the notations (17), we may write

$$A_{h,k} = D^{-1} B \Gamma_k M^{-1} B^T, \qquad C_{h,k} = D^{-1} B \Gamma_k M^{-1} G_h, \tag{58}$$

so that

$$Q_{h,k} = -A_{h,k} P_h + F_{h,k} + C_{h,k}.$$

According to (57), it is easy to see that

$$A_h = \sum_{k=1}^{m} A_{h,k}, \qquad C_h = \sum_{k=1}^{m} C_{h,k}.$$

As a result, the system of ordinary differential equations (18a) can be expressed as a split system of the form

$$P_h' + \sum_{k=1}^{m} A_{h,k} P_h = \sum_{k=1}^{m} L_{h,k}, \tag{59}$$

where $L_{h,k} = F_{h,k} + C_{h,k}$. If M is non-symmetric, a change of variable of the form $\check{P}_h = D^{1/2} P_h$ yields

$$\check{P}_h' + \sum_{k=1}^{m} \check{A}_{h,k} \check{P}_h = \sum_{k=1}^{m} \check{L}_{h,k}, \tag{60}$$

where $\check{A}_{h,k} = D^{-1/2} B \Gamma_k M^{-1} B^T D^{-1/2}$ and $\check{L}_{h,k} = D^{1/2} L_{h,k}$.

Lemma 7. *The matrices* $\{A_{h,k}\}_{k=1}^m$ *and* $\{\check{A}_{h,k}\}_{k=1}^m$, *associated to the split systems* (59) *and* (60), *respectively, satisfy*

$$\xi^T A_{h,k}\xi \geqslant 0 \quad \forall \xi \in \mathbb{R}^{N_e}, \tag{61a}$$

$$\eta^T \check{A}_{h,k}\eta \geqslant 0 \quad \forall \eta \in \mathbb{R}^{N_e}, \tag{61b}$$

for $k = 1, 2, \ldots, m$.

Proof. Since M is block-diagonal with blocks M_i, so is $\Gamma_k M^{-1}$ with blocks $\rho_k(\mathbf{r}_i)M_i^{-1}$, for $i = 1, 2, \ldots, N_v$ and $k = 1, 2, \ldots, m$. In both cases, such blocks are non-negative definite. Hence, using (20), $N_k = B\Gamma_k M^{-1}B^T$ is also a non-negative definite matrix. The handling of D^{-1} is as follows. If M is symmetric, so is N_k. Thus, for any $\xi \in \mathbb{R}^{N_e}$, if we consider $\theta = D^{-1/2}\xi$, we get

$$\xi^T D^{-1} N_k \xi = \theta^T D^{-1/2} N_k D^{1/2} \theta \geqslant 0,$$

which follows from the Rayleigh quotient, since $D^{-1/2}N_k D^{1/2}$ is similar to N_k. This result implies (61a). On the other hand, if M is non-symmetric, we consider the split system (60) and note that, for any $\xi \in \mathbb{R}^{N_e}$,

$$\xi^T D^{-1/2} N_k D^{-1/2} \xi = \theta^T N_k \theta \geqslant 0,$$

provided that $\theta = D^{-1/2}\xi$. Therefore, (61b) follows. □

A natural way to solve either (59) or (60) is the use of a fractional step time integrator which takes advantage of the multiterm partitioning. Since the discrete diffusion suboperators $\{A_{h,k}\}_{k=1}^m$ and $\{\check{A}_{h,k}\}_{k=1}^m$ do not commute pairwise, we further require a scheme whose stability is not affected by the lack of commutativity of the split terms. In the sequel, we present a family of fractional step methods which are defined to be unconditionally stable even in the non-commuting case.

5.2. The fully discrete scheme

In this subsection, we describe in detail the time integration of the split system (59); the procedure for (60) is similar. Let us consider an FSRK$_m$ method with s internal stages to integrate in time (59), with initial condition $P_h(0) = P_h^0$, i.e.,

$$\begin{cases} \text{For } n = 0, 1, \ldots, N_T\text{:} \\ \quad \text{For } k = 1, 2, \ldots, s\text{:} \\ \qquad P_h^{n,k} = P_h^n + \tau \displaystyle\sum_{\ell=1}^{k} a_{k\ell}^{i_\ell}\big(-A_{h,i_\ell} P_h^{n,\ell} + L_{h,i_\ell}(t_{n,\ell})\big), \\ \qquad P_h^{n+1} = P_h^n + \tau \displaystyle\sum_{\ell=1}^{s} b_\ell^{i_\ell}\big(-A_{h,i_\ell} P_h^{n,\ell} + L_{h,i_\ell}(t_{n,\ell})\big), \end{cases} \tag{62}$$

where P_h^n is an approximation to the solution of (59) at $t = t_n$. For the sake of simplicity in the exposition, the time step τ is considered to be constant, $t_n = n\tau$ and $N_T \equiv [T/\tau] - 1$. Moreover, $i_\ell \in \{1, 2, \ldots, m\}$ and $t_{n,\ell} = t_n + c_\ell \tau$, for $\ell = 1, 2, \ldots, s$. The choice of different coefficients $a_{k\ell}^j$, b_ℓ^j and c_ℓ determines each particular FSRK$_m$ method, where $1 \leqslant \ell \leqslant k \leqslant s$ for $j = 1, 2, \ldots, m$.

Note that i_k denotes the part of the discrete operator A_h which acts implicitly at the kth internal stage, and it is also given by the method under consideration. A specific choice for i_k is given below. For $k = 1, 2, \ldots, s$, the linear system to solve is

$$\big(I + \tau a_{kk}^{i_k} A_{h,i_k}\big) P_h^{n,k} = S_h^{n,k}, \tag{63}$$

where $i_k \in \{1, 2, \ldots, m\}$. In this case, I denotes the identity matrix and $S_h^{n,k}$ stands for the corresponding right-hand side. Since $\operatorname{supp}(\rho_{i_k}(\mathbf{x})) \subset \overline{\Omega}_{i_k}$, the entries of A_{h,i_k} are zeroes outside $\overline{\Omega}_{i_k}$. Further, as Ω_{i_k} involves m_{i_k} disjoint connected components, namely $\Omega_{i_k l}$, the linear system (63) is indeed a collection of m_{i_k} uncoupled subsystems of the form

$$\big(I_{\Omega_{i_k l}} + \tau a_{kk}^{i_k} A_{h,\Omega_{i_k l}}\big)\mathcal{R}_{\Omega_{i_k l}} P_h^{n,k} = \mathcal{R}_{\Omega_{i_k l}} S_h^{n,k}, \tag{64}$$

where $I_{\Omega_{i_k l}} = \mathcal{R}_{\Omega_{i_k l}} I \mathcal{R}_{\Omega_{i_k l}}^T$ and $A_{h,\Omega_{i_k l}} = \mathcal{R}_{\Omega_{i_k l}} A_{h,i_k} \mathcal{R}_{\Omega_{i_k l}}^T$, $\mathcal{R}_{\Omega_{i_k l}}$ being a restriction matrix from Ω to $\Omega_{i_k l}$, as defined in Remark 1 below. Unlike most classical domain decomposition algorithms (cf. [29]), the solution to (64) does not require any Schwarz iteration procedure, since the internal stages in (62) are solved sequentially (i.e., interface conditions need not be imposed on subdomains during the solution process).

Remark 1. The rectangular matrices $\mathcal{R}_{\Omega_{kl}}$ and $\mathcal{R}^T_{\Omega_{kl}}$ are usually called restriction and extension mappings, respectively, and represent a type of domain decomposition preconditioners. Formally, let N and N_s be the number of total unknowns in Ω and Ω_{kl}, respectively. Let us further define an index function $\text{index}(\Omega_{kl}, i)$ to denote the global index of the ith local unknown in Ω_{kl}, for $i = 1, 2, \ldots, N_s$. Then, the restriction matrix $\mathcal{R}_{\Omega_{kl}} \in \mathbb{R}^{N_s \times N}$ is defined to be

$$(\mathcal{R}_{\Omega_{kl}})_{ij} = \begin{cases} 1, & \text{if } \text{index}(\Omega_{kl}, i) = j, \\ 0, & \text{if } \text{index}(\Omega_{kl}, i) \neq j. \end{cases}$$

This matrix restricts a vector $\mathbf{v} \in \mathbb{R}^N$, whose components are associated to the mesh cells in Ω, to a vector $\mathcal{R}_{\Omega_{kl}}\mathbf{v} \in \mathbb{R}^{N_s}$ with components in Ω_{kl} (using the local ordering). Likewise, the transpose matrix $\mathcal{R}^T_{\Omega_{kl}} \in \mathbb{R}^{N \times N_s}$ extends a vector $\mathbf{v}_{\Omega_{kl}} \in \mathbb{R}^{N_s}$ with components in Ω_{kl} to a vector $\mathcal{R}^T_{\Omega_{kl}}\mathbf{v}_{\Omega_{kl}} \in \mathbb{R}^N$ with components in Ω, inserting zero entries for the global indices which do not belong to Ω_{kl}. Note that, given a global matrix $S \in \mathbb{R}^{N \times N}$, its submatrix $S_{\Omega_{kl}} \in \mathbb{R}^{N_s \times N_s}$ corresponding to the mesh cells in Ω_{kl} may be obtained from the restriction and extension mappings as $S_{\Omega_{kl}} = \mathcal{R}_{\Omega_{kl}} S \mathcal{R}^T_{\Omega_{kl}}$ (cf. [23]).

In the sequel, we introduce a specific family of FSRK$_m$ methods of the form (62). These methods are formulated for an arbitrary number m of implicit parts, what makes them likely to be combined with an operator splitting into an arbitrary number m of split terms. Such terms are not required to commute pairwise and, thus, the newly introduced schemes preserve a rather general splitting framework.

In particular, the fully discrete MFMFE–FSRK$_m$ scheme reads

$$\begin{cases} \text{For } n = 0, 1, \ldots, N_T\text{:} \\ \quad P_h^{n,1} = P_h^n, \\ \quad \text{For } k = 2, 3, \ldots, 2m-1\text{:} \\ \qquad P_h^{n,k} = P_h^{n,k-1} + \tau \displaystyle\sum_{\ell=k-1}^{k} \alpha_\ell \left(-A_{h,i_\ell} P_h^{n,\ell} + L_{h,i_\ell}(t_{n,\ell})\right), \\ \quad P_h^{n+1} = P_h^{n,2m-1}, \end{cases} \tag{65}$$

where $\alpha_k = \frac{1}{2}$, for $k \in \{1, m, 2m-1\}$, and $\alpha_k = \frac{1}{4}$, otherwise; accordingly, $i_k = k$, for $k = 1, 2, \ldots, m$, and $i_k = 2m - k$, otherwise. In turn, the intermediate times are $t_{n,1} = t_n$, $t_{n,k} = t_n + \frac{\tau}{2}$, for $k = 2, 3, \ldots, 2m-2$, and $t_{n,2m-1} = t_{n+1}$.

In this case, the linear system to solve at the kth internal stage is given by (63), with $a^{i_k}_{kk} = \alpha_k$ and the right-hand side

$$S_h^{n,k} = (I - \tau\alpha_{k-1} A_{h,i_{k-1}}) P_h^{n,k-1} + \tau\left(\alpha_{k-1} L_{h,i_{k-1}}(t_{n,k-1}) + \alpha_k L_{h,i_k}(t_{n,k})\right),$$

where $i_k \in \{1, 2, \ldots, m\}$, for $k = 2, 3, \ldots, 2m-1$. As in the general case, such a system may be decomposed into m_{i_k} uncoupled subsystems of the form (64). This family of time integrators was first proposed in [25] as a variant of the classical two-cycle scheme (cf. [39]), which reduces by two the number of internal stages while preserving its accuracy. In addition, as mentioned above, the Peaceman–Rachford ADI method is a particular instance of the scheme (65), if $m = 2$ and $A_{h,k}$, for $k = 1, 2$, are suitable discretizations of one-dimensional differential operators with respect to x and y, respectively.

Remark 2. From a computational viewpoint, in order to minimize the number of sequential steps (i.e., internal stages) in the algorithm (65), the number of subdomains m should be chosen to be as small as possible. Additionally, to ensure that the loads assigned to each processor are balanced, there should be approximately the same number of connected components m_k in each subdomain Ω_k and, moreover, each such component should be approximately of the same diameter. For instance, suppose that we have q processors available for parallel computing. Then, if the number of connected components m_k is approximately the same in each subdomain Ω_k and also a multiple of q, each such component can be partitioned into q groups of $\frac{m_k}{q}$ components and each group assigned to one of the processors.

6. Error analysis of the fully discrete scheme

In this section, we describe the convergence analysis of the fully discrete scheme (65). In doing so, we extend the results in [30] for the Peaceman–Rachford ADI method applied to linear problems (i.e., (65) with $m = 2$) to a domain decomposition splitting formula into an arbitrary number of split terms ($m \geqslant 2$).

Let us define the full discretization error at t_{n+1} as the difference $\bar{p}_h(t_{n+1}) - P_h^{n+1}$, where

$$\bar{p}_h(t) = r_h\left(\mathcal{P}_h p(\mathbf{x}, t)\right).$$

Here, $r_h : W_h \to \mathcal{H}_p$ denotes the restriction operator of the scalar functions in W_h to the cell centers of $\mathcal{T}_h$. This global error can be analyzed via two different approaches.

The first one considers the following decomposition

$$\bar{p}_h(t_{n+1}) - P_h^{n+1} = \big(\bar{p}_h(t_{n+1}) - P_h(t_{n+1})\big) + \big(P_h(t_{n+1}) - P_h^{n+1}\big).$$

In this case, the former difference on the right-hand side represents a spatial semidiscretization error, and is bounded above by Theorem 6 for the symmetric MFMFE method. In order to derive a bound for the latter difference, it would be necessary to estimate the derivatives of the semidiscrete solution $P_h(t)$.

To overcome this requirement, we take an alternative approach based on the method of lines (cf. [40–42]). The full discretization error is decomposed into the sum

$$\bar{p}_h(t_{n+1}) - P_h^{n+1} = \big(\bar{p}_h(t_{n+1}) - \hat{P}_h^{n+1}\big) + \big(\hat{P}_h^{n+1} - P_h^{n+1}\big), \tag{66}$$

where $\hat{P}_h^{n+1}$ denotes the numerical solution obtained when applying the method with a time step τ and the initial value $P_h^n = \bar{p}_h(t_n)$. The difference

$$\beta_h^{n+1} = \bar{p}_h(t_{n+1}) - \hat{P}_h^{n+1}$$

is commonly known as the full truncation error at t_{n+1}. In the sequel, we shall describe in detail how to derive suitable bounds for the global error based on (66).

Throughout this section, $(\cdot,\cdot)_{\ell^2}$ stands for the discrete L^2-inner product in $\mathcal{H}_p$ and $\|\cdot\|_{\ell^2} = (\cdot,\cdot)_{\ell^2}^{1/2}$ is the induced discrete L^2-norm. Note that, for any $w \in W_h$, the continuous and discrete L^2-norms can be related via the restriction operator r_h, i.e.,

$$\|r_h w\|_{\ell^2} = \|w\| \quad \forall w \in W_h. \tag{67}$$

6.1. Stability

In order to study the stability of the fully discrete scheme (65), let us consider the perturbed scheme

$$\begin{cases} \tilde{P}_h^0 = P_h^0 + \varepsilon_h^0, \\ \text{For } n = 0, 1, \ldots, N_T: \\ \quad \tilde{P}_h^{n,1} = \tilde{P}_h^n, \\ \quad \text{For } k = 2, 3, \ldots, 2m-1: \\ \qquad \tilde{P}_h^{n,k} = \tilde{P}_h^{n,k-1} + \tau \displaystyle\sum_{\ell=k-1}^{k} \alpha_\ell\big(-A_{h,i_\ell}\tilde{P}_h^{n,\ell} + L_{h,i_\ell}(t_{n,\ell})\big) + \tau\delta_h^{n,k}, \\ \quad \tilde{P}_h^{n+1} = \tilde{P}_h^{n,2m-1}, \end{cases} \tag{68}$$

where ε_h^0 denotes the error in the initial data, and $\delta_h^{n,k}$ may stand for round-off errors, errors due to non-exactly solving the implicit relations or discretization errors. Let us define, for $n = 0, 1, \ldots, N_T$,

$$\varepsilon_h^{n+1} = \tilde{P}_h^{n+1} - P_h^{n+1}. \tag{69}$$

Subtracting (65) from (68), we may write

$$\varepsilon_h^{n+1} = R_h\left(I - \tfrac{\tau}{2}A_{h,1}\right)\varepsilon_h^n + \tau\sum_{k=2}^{2m-1} S_h^k\delta_h^{n,k}, \tag{70}$$

where

$$R_h \equiv \big(I + \tfrac{\tau}{2}A_{h,1}\big)^{-1} T_h^{2m-2}T_h^{2m-3}\cdots T_h^2, \tag{71a}$$

$$S_h^{2m-1} \equiv \big(I + \tfrac{\tau}{2}A_{h,1}\big)^{-1}, \tag{71b}$$

$$S_h^k \equiv \big(I + \tfrac{\tau}{2}A_{h,1}\big)^{-1} T_h^{2m-2}T_h^{2m-3}\cdots T_h^k, \quad \text{for } k = 2, 3, \ldots, 2m-2, \tag{71c}$$

$$T_h^\ell \equiv (I - \tau\alpha_\ell A_{h,i_\ell})(I + \tau\alpha_\ell A_{h,i_\ell})^{-1}, \quad \text{for } \ell = 2, 3, \ldots, 2m-2. \tag{71d}$$

In the sequel, we quote two auxiliary results that will be used below to analyze the stability of the fully discrete scheme.

Lemma 8. *Let $\Lambda \in \mathbb{R}^{s\times s}$, for $s \in \mathbb{N}$, satisfy*

$$\xi^T\Lambda\xi \geqslant 0 \quad \forall \xi \in \mathbb{R}^s, \tag{72a}$$

$$\xi^T\Lambda^T\Lambda\xi \leqslant \alpha\xi^T\xi \quad \forall \xi \in \mathbb{R}^s, \tag{72b}$$

where α is a positive constant. Then, for any $\mu > 0$, it holds

$$\left\|(I+\mu\Lambda)^{-1}\right\|_2 \leqslant 1, \tag{73a}$$

$$\left\|(I-\mu\Lambda)(I+\mu\Lambda)^{-1}\right\|_2 \leqslant 1, \tag{73b}$$

$$\left\|\mu\Lambda(I+\mu\Lambda)^{-1}\right\|_2 \leqslant C, \tag{73c}$$

where C is a positive constant and $\|\cdot\|_2$ denotes the spectral norm.

Proof. In order to prove the first inequality, it is not difficult to see that, due to (72a),

$$\xi^T\xi \leqslant \xi^T\left(I+\mu\Lambda^T\right)(I+\mu\Lambda)\xi.$$

Thus, making the substitution $\xi = (I+\mu\Lambda)^{-1}\eta$, we obtain (73a) and complete the proof. As for the second inequality, the previous argument yields

$$\xi^T\left(I-\mu\Lambda^T\right)(I-\mu\Lambda)\xi \leqslant \xi^T\left(I+\mu\Lambda^T\right)(I+\mu\Lambda)\xi.$$

In this case, (73b) follows upon the same substitution for ξ. Accordingly, (72a) implies that

$$\mu^2\xi^T\Lambda^T\Lambda\xi \leqslant \mu^2\xi^T\left(I+\mu\Lambda^T\right)\Lambda^T\Lambda(I+\mu\Lambda)\xi.$$

The inequality (73c) is then derived by taking $\xi = (I+\mu\Lambda)^{-1}\eta$ and using (72b). □

Since the split matrices $\{A_{h,k}\}_{k=1}^m$ lie in the framework of Lemma 8, the inequalities (73) can be used to derive the following result.

Lemma 9. *Let $\{A_{h,k}\}_{k=1}^m$ be the matrices defined in (58). Then, for any $\tau > 0$, $q \in \mathbb{N}$ and $k = 2, 3, \ldots, 2m-1$, it holds*

$$\left\|\left(R_h\left(I-\tfrac{\tau}{2}A_{h,1}\right)\right)^q\phi\right\|_{\ell^2} \leqslant \left\|\left(I-\tfrac{\tau}{2}A_{h,1}\right)\phi\right\|_{\ell^2}, \tag{74a}$$

$$\left\|\left(R_h\left(I-\tfrac{\tau}{2}A_{h,1}\right)\right)^q S_h^k\phi\right\|_{\ell^2} \leqslant \|\phi\|_{\ell^2}. \tag{74b}$$

Proof. Recalling the definition (71a), the left-hand side of (74a) can be expanded to get

$$\left\|\left(I+\tfrac{\tau}{2}A_{h,1}\right)^{-1}T_h^{2m-2}\cdots T_h^2T_h^1T_h^{2m-2}\cdots T_h^2\left(I-\tfrac{\tau}{2}A_{h,1}\right)\phi\right\|_{\ell^2} \leqslant \left\|\left(I-\tfrac{\tau}{2}A_{h,1}\right)\phi\right\|_{\ell^2},$$

where (73a) and (73b), with $\Lambda = A_{h,k}$, do apply. Accordingly, (74b) is derived from (71a)–(71c), also taking into account (73a) and (73b). □

The following stability result for the MFMFE–FSRK$_m$ scheme (65) is thus obtained.

Theorem 7. *Let ε_h^{n+1} be defined by (69). If the matrices $\{A_{h,k}\}_{k=1}^m$ are given by (58), then it holds, for $n = 0, 1, \ldots, N_T$,*

$$\left\|\varepsilon_h^{n+1}\right\|_{\ell^2} \leqslant \left\|\left(I-\tfrac{\tau}{2}A_{h,1}\right)\varepsilon_h^0\right\|_{\ell^2} + C\max_{\substack{0\leqslant j\leqslant n\\ 2\leqslant k\leqslant 2m-1}}\left\|\delta_h^{j,k}\right\|_{\ell^2}, \tag{75}$$

where C is a positive constant, defined to be independent of h and τ.

Proof. Expanding the recurrence relation (70), we obtain

$$\varepsilon_h^{n+1} = \left(R_h\left(I-\tfrac{\tau}{2}A_{h,1}\right)\right)^{n+1}\varepsilon_h^0 + \tau\sum_{j=0}^{n}\sum_{k=2}^{2m-1}\left(R_h\left(I-\tfrac{\tau}{2}A_{h,1}\right)\right)^{n-j}S_h^k\delta_h^{j,k}.$$

Hence, (75) follows from the triangle inequality and the bounds (74). □

The previous bound expresses stability of the fully discrete scheme with respect to the transformed initial error $\hat{\varepsilon}_h^0 = (I - \frac{\tau}{2}A_{h,1})\varepsilon_h^0$ and the original perturbations $\delta_h^{j,k}$, for $j = 0, 1, \ldots, n$ and $k = 2, 3, \ldots, 2m-1$. As a consequence, if $\|\hat{\varepsilon}_h^0\|_{\ell^2} \leqslant C\|\varepsilon_h^0\|_{\ell^2}$, with $C > 0$ independent of h, then (75) shows unconditional stability[2] with respect to the initial error ε_h^0 and the perturbations $\delta_h^{j,k}$. In general, $\hat{\varepsilon}_h^0$ can be viewed as the difference of two forward Euler steps, i.e.,

$$\hat{\varepsilon}_h^0 = \big(\tilde{P}_h^0 - \tfrac{\tau}{2}A_{h,1}\tilde{P}_h^0\big) - \big(P_h^0 - \tfrac{\tau}{2}A_{h,1}P_h^0\big).$$

Thus, we may have $\|\hat{\varepsilon}_h^0\|_{\ell^2} \gg \|\varepsilon_h^0\|_{\ell^2}$, because of the explicitness of the previous expression. In [30], the authors propose a technique to stabilize the first step of the Peaceman–Rachford ADI method that would also apply to our scheme. Nonetheless, as they point out, there seems to be no need for such a stabilization from a practical viewpoint.

6.2. Consistency

To study the consistency of the scheme, we consider the perturbed scheme (68) and let $\tilde{P}_h^n = \bar{p}_h(t_n)$ and $\tilde{P}_h^{n,k} = \bar{p}_h(t_{n,k})$, for $k = 1, 2, \ldots, 2m-1$. As a result, $\tilde{P}_h^{n+1} = \bar{p}_h(t_{n+1})$ and (69) represents the full discretization error at t_{n+1}, i.e.,

$$\varepsilon_h^{n+1} = \bar{p}_h(t_{n+1}) - P_h^{n+1}.$$

Since $\hat{P}_h^{n+1}$ denotes the numerical solution obtained in one single step of (65) starting at $P_h^n = \bar{p}_h(t_n)$, we have that $\hat{P}_h^{n+1} - P_h^{n+1} = R_h(I - \frac{\tau}{2}A_{h,1})\varepsilon_h^n$ and the relation (66) can be expressed as

$$\varepsilon_h^{n+1} = R_h\big(I - \tfrac{\tau}{2}A_{h,1}\big)\varepsilon_h^n + \beta_h^{n+1}. \tag{76}$$

A term-by-term comparison of (70) and (76) yields the following expression for the full truncation error

$$\beta_h^{n+1} = \tau \sum_{k=2}^{2m-1} S_h^k \delta_h^{n,k}, \tag{77}$$

where $\delta_h^{n,k}$ are defined from (68) with the choice $\tilde{P}_h^n = \bar{p}_h(t_n)$.

For later use, we define the spatial truncation error $\alpha_h(t)$ as given by

$$\alpha_h(t) = \bar{p}_h'(t) + A_h\bar{p}_h(t) - L_h(t), \quad t \in [0, T], \tag{78}$$

where $\bar{p}_h'(t) = r_h(\mathcal{P}_h p_t(\mathbf{x}, t))$ and $L_h(t) = F_h(t) + C_h(t)$.

Within this framework, we can derive the following consistency result.

Theorem 8. *Let $\bar{p}_h(t)$ fulfill, for all $t \in [t_n, t_{n+1}]$,*

$$\big\|\bar{p}_{h,k}'''(t)\big\|_{\ell^2} \leqslant C, \tag{79a}$$

$$\big\|\Lambda_1\bar{p}_{h,k}''(t)\big\|_{\ell^2} \leqslant C, \tag{79b}$$

$$\big\|\Lambda_1\Lambda_2\bar{p}_{h,k}'(t)\big\|_{\ell^2} \leqslant C, \tag{79c}$$

where $\bar{p}_{h,k}'(t) = L_{h,k}(t) - A_{h,k}\bar{p}_h(t)$ and $\Lambda_j \in \{A_{h,1}, A_{h,2}, \ldots, A_{h,m}\}$, for $k = 1, 2, \ldots, m$ and $j = 1, 2$. Then, the full truncation error β_h^{n+1} satisfies, for $m \geqslant 2$ and $n = 0, 1, \ldots, N_T$,

$$\big\|\beta_h^{n+1}\big\|_{\ell^2} \leqslant C\big(\tau^3 + \tau\big\|\alpha_h(t_{n+1/2})\big\|_{\ell^2}\big) \quad \forall\tau \in (0, \tau_0], \tag{80}$$

where C is a positive constant, defined to be independent of h and τ.

Proof. Let $\tilde{P}_h^n = \bar{p}_h(t_n)$ and $\tilde{P}_h^{n,k} = \bar{p}_h(t_{n,k})$, for $k = 1, 2, \ldots, 2m-1$, in (68). Initially, we consider Taylor expansions of $\bar{p}_h$ and $-A_{h,k}\bar{p}_h + L_{h,k}$ around $t = t_{n+1/2}$. Evaluating the spatial truncation error (78) at this same point and inserting the split terms, we get

$$\alpha_h(t_{n+1/2}) = \bar{p}_h'(t_{n+1/2}) + \sum_{k=1}^{m}\big(A_{h,k}\bar{p}_h(t_{n+1/2}) - L_{h,k}(t_{n+1/2})\big).$$

[2] This happens, for instance, whenever $\varepsilon_h^0 = 0$ or ε_h^0 is a smooth grid function, so that $\|A_{h,1}\varepsilon_h^0\|_{\ell^2} \leqslant C'\|\varepsilon_h^0\|_{\ell^2}$.

This relation, together with (79a), yields the following expressions for $\delta_h^{n,k}$

$$\delta_h^{n,2} = \tau\, w_h(t_{n+1/2}) + \sum_{k=2}^{m-1} v_{k,h}(t_{n+1/2}) + \tfrac{1}{2}\alpha_h(t_{n+1/2}) + \mathcal{O}(\tau^2), \tag{81a}$$

$$\delta_h^{n,k+1} = -v_{k,h}(t_{n+1/2}), \quad \text{for } k = 2, 3, \ldots, m-1, \tag{81b}$$

$$\delta_h^{n,2m-k} = -v_{k,h}(t_{n+1/2}), \quad \text{for } k = m-1, m-2, \ldots, 2, \tag{81c}$$

$$\delta_h^{n,2m-1} = -\tau\, w_h(t_{n+1/2}) + \sum_{k=2}^{m-1} v_{k,h}(t_{n+1/2}) + \tfrac{1}{2}\alpha_h(t_{n+1/2}) + \mathcal{O}(\tau^2), \tag{81d}$$

where

$$w_h(t) = -\tfrac{1}{8}\bar{p}_h''(t) + \tfrac{1}{4}\bar{p}_{h,1}''(t), \qquad v_{k,h}(t) = \alpha_k \bar{p}_{h,k}'(t) + \alpha_{k+1}\bar{p}_{h,k+1}'(t).$$

Recall that $\{\alpha_k\}_{k=2}^m$ denote the coefficients of the fully discrete scheme (65) with values $\alpha_2 = \alpha_3 = \cdots = \alpha_{m-1} = \frac{1}{4}$ and $\alpha_m = \frac{1}{2}$. Inserting the expressions (81) into the definition (77) of the full truncation error, we get

$$\beta_h^{n+1} = \sum_{\ell=2}^{2m-2} S_h^{\ell+1}(I + \tau\alpha_\ell A_{h,i_\ell})^{-1}\Big(\tau a_\ell \alpha_h(t_{n+1/2}) + \tau^2 b_\ell A_{h,i_\ell}\alpha_h(t_{n+1/2}) + \tau^3 c_\ell A_{h,i_\ell} w_h(t_{n+1/2}) + \tau^3 \sum_{j,k\in\{2,\ldots,m-1\}} d_{jk\ell} A_{h,i_\ell} A_{h,j} v_{k,h}(t_{n+1/2})\Big) + \mathcal{O}(\tau^3), \tag{82}$$

where a_ℓ, b_ℓ, c_ℓ and $d_{jk\ell}$ are certain coefficients (some of them equal to zero). Finally, the application of bounds (73), with $\Lambda = A_{h,k}$, (79b) and (79c) implies (80) and completes the proof. □

Conditions of type (79) are derived in [19]. In this work, the authors prove similar bounds for a standard 5-point finite difference approximation to $-\nabla\cdot(\rho_k K\nabla p)$ in two-dimensional parabolic problems with homogeneous Dirichlet boundary data. The extension of these results to the MFMFE method is based on the following idea. Recall that the partitioned discrete diffusion term is given by $B\Gamma_k M^{-1}B^T P_h$. Here, $B^T P_h$ involves first-order differences in pressures, so that $M^{-1}B^T P_h$ is a linear combination of pressure differences, whose coefficients contain the elements of tensor K evaluated at the vertex points. This term represents an approximation to the negative flux, $K\nabla p$. Since B provides an extra level of first-order differences, $B\Gamma_k M^{-1}B^T P_h$ becomes a 9-point stencil approximation to $-\nabla\cdot(\rho_k K\nabla p)$ on logically rectangular grids. The procedure in [19] can then be applied.

Let us now examine the hypotheses (79) in more detail. On the one hand, (79a) is satisfied provided that $p(\mathbf{x}, t)$ is a smooth function and the problem data are sufficiently smooth and compatible. However, (79b) and (79c) are somehow non-natural conditions, since, in general, they are not in accordance with the preceding smoothness and compatibility requirements. This fact is illustrated in [42] for the case of a standard finite difference discretization of the one-dimensional heat equation on a uniform grid. If homogeneous Dirichlet boundary conditions are considered, and the source term f and its even spatial derivatives up to certain order vanish at the boundary, then (79b) and (79c) are satisfied. Otherwise, some order reduction may occur in the full truncation error.

These considerations imply that, if we assumed (79a) as the only hypothesis of Theorem 8, we would obtain

$$\|\beta_h^{n+1}\|_{\ell^2} \leqslant C\big(\tau^{q+1} + \tau\,\|\alpha_h(t_{n+1/2})\|_{\ell^2}\big) \tag{83}$$

instead of (80), where q is the so-called stage order. The value of the stage order equals 1, if $m = 2$, and 0, otherwise. For the case $m = 2$, it is easy to deduce from (82) that the full truncation error admits the expression

$$\beta_h^{n+1} = \big(I + \tfrac{\tau}{2}A_{h,1}\big)^{-1}\big(I + \tfrac{\tau}{2}A_{h,2}\big)^{-1}\big(-\tau^3 A_{h,2} w_h(t_{n+1/2}) + \tau\alpha_h(t_{n+1/2})\big) + \mathcal{O}(\tau^3).$$

Taking into account the uniform boundedness of $w_h(t)$, together with the bounds (73a) and (73c), with $\Lambda = A_{h,1}$ and $\Lambda = A_{h,2}$, respectively, the consistency result (83) follows for a value $q = 1$. This idea can be easily extended to derive the corresponding bounds for higher values of m.

Remark 3. In the framework of Runge–Kutta methods for linear parabolic problems, the order reduction phenomenon was first studied in [43,44], and has been subsequently analyzed in [41,42,45–47], among others. This subject is further investigated in [48,49,30,50] in the context of splitting methods. In particular, [50] studies the order reduction of FSRK$_m$ methods and proposes a technique to avoid it. Such a technique, based on suitably modifying the boundary values of the internal stages, is used in [25] to avoid the order reduction of scheme (65) when alternating direction operator splittings are considered.

6.3. Convergence

The convergence of the fully discrete scheme (65) follows from the preceding results on stability and consistency. Throughout this section, we shall make use of the notation

$$\|\bar{p}_h - P_h\|_{\ell^\infty(\ell^2)} = \max_{0\leqslant n\leqslant N_T} \left\|\bar{p}_h(t_{n+1}) - P_h^{n+1}\right\|_{\ell^2}$$

for the global error of the MFMFE–FSRK$_m$ method.

Theorem 9. *Under the hypotheses of Theorem 8, the fully discrete solution P_h^{n+1} of the MFMFE–FSRK$_m$ method (65), with $\{A_{h,k}\}_{k=1}^m$ given by (58), satisfies*

$$\|\bar{p}_h - P_h\|_{\ell^\infty(\ell^2)} \leqslant C\left(\tau^2 + \max_{0\leqslant t\leqslant T}\left\|\alpha_h(t)\right\|_{\ell^2}\right), \tag{84}$$

where C is a positive constant, independent of h and τ.

Proof. Expanding the recurrence relation (76), we get

$$\varepsilon_h^{n+1} = \left(R_h\left(I - \tfrac{\tau}{2}A_{h,1}\right)\right)^{n+1}\varepsilon_h^0 + \sum_{j=1}^{n+1}\left(R_h\left(I - \tfrac{\tau}{2}A_{h,1}\right)\right)^{n+1-j}\beta_h^j. \tag{85}$$

Note that $\varepsilon_h^0 = 0$ since $P_h^0 = r_h(\mathcal{P}_h p_0(\mathbf{x}))$, and the first term on the right-hand side vanishes. As for the second term, we consider the expression (82) for the full truncation errors, and further use (74b), (73a) and (73c), with $\Lambda = A_{h,k}$, (79b) and (79c). This yields

$$\left\|\varepsilon_h^{n+1}\right\|_{\ell^2} \leqslant \sum_{j=1}^{n+1} C\left(\tau^3 + \tau\left\|\alpha_h(t_{j-1/2})\right\|_{\ell^2}\right) \leqslant C\left(\tau^2 + \max_{0\leqslant t\leqslant T}\left\|\alpha_h(t)\right\|_{\ell^2}\right).$$

The inequality (84) is finally obtained by taking the maximum over n. □

Remark 4. The local truncation error for MPFA methods is mainly studied in [12,51–53]. In these works, such an error is shown to be second-order convergent for the pressure variable in the case of rectangular grids. Via a smooth mapping, this result can be extended to the symmetric version of the MFMFE method on hexahedral grids. The thesis of Theorem 9 thus implies

$$\|\bar{p}_h - P_h\|_{\ell^\infty(\ell^2)} \leqslant C\left(h^2 + \tau^2\right).$$

If we further define p_h^{n+1} as the element of W_h such that $r_h p_h^{n+1} = P_h^{n+1}$, we may write

$$\left\|p(t_{n+1}) - p_h^{n+1}\right\| \leqslant \left\|p(t_{n+1}) - \mathcal{P}_h p(t_{n+1})\right\| + \left\|r_h\left(\mathcal{P}_h p(t_{n+1})\right) - P_h^{n+1}\right\|_{\ell^2},$$

where (67) applies. Since $\|p - \mathcal{P}_h p\| \leqslant Ch|p|_1$ (cf. [1,5]), it follows that the previous expression is $\mathcal{O}(h + \tau^2)$. Finally, taking the maximum over n yields, with an abuse of notation,

$$\|p - p_h\|_{\ell^\infty(L^2)} = \max_{0\leqslant n\leqslant N_T}\left\|p(t_{n+1}) - p_h^{n+1}\right\| \leqslant C\left(h + \tau^2\right). \tag{86}$$

In virtue of (83), if we just considered the assumption (79a) in Theorem 8, we would expect to obtain

$$\left\|\varepsilon_h^{n+1}\right\|_{\ell^2} \leqslant C\left(\tau^q + \max_{0\leqslant t\leqslant T}\left\|\alpha_h(t)\right\|_{\ell^2}\right),$$

as a result of the addition of all the truncation errors. However, cancellation of such errors may occur, thus leading to an exponent $q+1$ for τ in the previous expression. This behavior can also be observed for some classical Runge–Kutta methods (see [41] and references therein). In [30], the authors recover the second-order convergence of the Peaceman–Rachford ADI method, assuming commutativity of the split operators. A similar argument could be used for the fully discrete scheme (65), in the case $m = 2$, if $\{A_{h,k}\}_{k=1}^2$ were commuting matrices. Nevertheless, as we shall illustrate in the next section, the second-order convergence is observed in practice even in the non-commuting case.

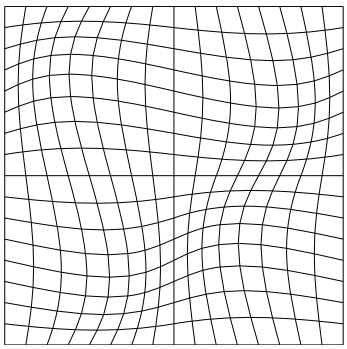

Fig. 3. Smooth quadrilateral mesh.

7. Numerical experiments

In the sequel, we illustrate the main features of the proposed methods by reporting a collection of convergence and scalability tests. In doing so, we obtain numerical results for both the pressure and velocity variables in different time–space norms. Note that, since the fully discrete scheme (65) is formulated in terms of pressures, the error analysis of the previous section does not provide error estimates for the flux variable. However, flux convergence rates may be obtained numerically by using the fully discrete counterpart of the expression (16). In addition, we show the suitability of the algorithms for the numerical solution of flow problems involving discontinuous permeability tensors.

7.1. Convergence and scalability tests

Let us consider problem (1) posed on the unit square, with t varying in $[0, 2]$ and tensor K given by

$$K(\mathbf{x}) = \begin{pmatrix} 4 + (x+2)^2 + y^2 & 1 + \sin(xy) \\ 1 + \sin(xy) & 2 \end{pmatrix}.$$

Data f, g and p_0 are chosen in such a way that

$$p(\mathbf{x}, t) = \frac{30 + 72t}{15 + 4096t^6} \sin(3\pi x)^2 \sin(3\pi y)^2$$

is the exact solution, and the boundary conditions are considered to be of Dirichlet type. The numerical solution of this problem follows the method of lines approach: we initially consider a spatial discretization based on the MFMFE method presented in Section 2, and subsequently apply a domain decomposition splitting technique along the lines of Section 5.

The spatial domain is discretized by means of three different types of quadrilateral meshes consisting of $N \times N$ elements. The first one is a family of smooth meshes composed of h^2-parallelograms, where $h = 1/N$. It is defined as a $\mathcal{C}^\infty$ mapping of successively refined uniform meshes on the unit square and presents the form

$$x = \hat{x} + \frac{3}{50} \sin(2\pi \hat{x}) \sin(2\pi \hat{y}),$$
$$y = \hat{y} - \frac{1}{20} \sin(2\pi \hat{x}) \sin(2\pi \hat{y}).$$

An illustration of this type of meshes is given in Fig. 3.

On the other hand, we consider a family of h-perturbed quadrilateral grids, whose construction is based on the definition of a primal mesh on the unit square. As shown in Fig. 4 (left), such a mesh consists of four congruent elements. The element located at the lower left position of the mesh is defined by the vertices $(0, 0)$, $(\frac{1}{2}, 0)$, $(\frac{1}{2}, \frac{3}{4})$ and $(0, \frac{1}{4})$. Thus, in order to construct the h-perturbed mesh shown in Fig. 4 (right), we first consider a uniform mesh on the unit square involving $N \times N$ elements, and subsequently apply suitable dilation and translation mappings of the primal mesh onto each of these elements (cf. [54,55]).

The third type of meshes is a family of randomly h-perturbed grids consisting of highly distorted quadrilaterals. Specifically, they are constructed by perturbing the vertices of a uniform mesh by a distance $\mathcal{O}(h)$ in a random direction. In particular, the vertices of the mesh displayed on Fig. 5 are obtained as

$$x_{i,j} = \hat{x}_{i,j} - \frac{5}{4}h + \frac{\sqrt{2}}{3} h r^x_{i,j},$$
$$y_{i,j} = \hat{y}_{i,j} - \frac{5}{4}h + \frac{\sqrt{2}}{3} h r^y_{i,j},$$

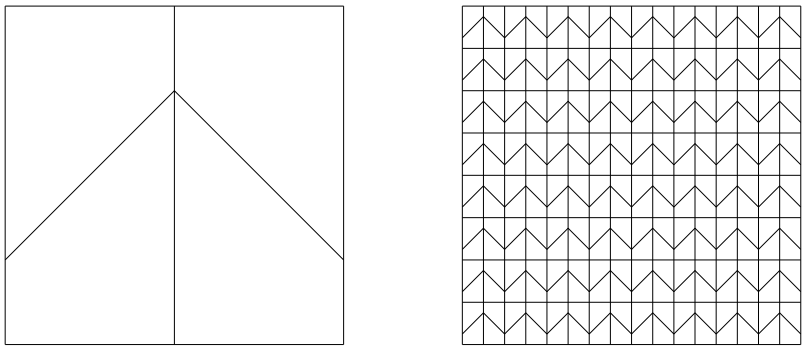

Fig. 4. Primal mesh on the unit square (left) and h-perturbed quadrilateral mesh (right).

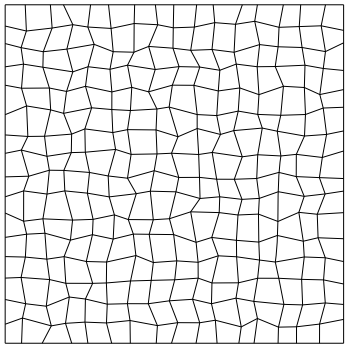

Fig. 5. Randomly h-perturbed quadrilateral mesh.

where $r^x_{i,j}$ and $r^y_{i,j}$ are pseudo-random numbers uniformly distributed in the interval $(0,1)$.

In order to keep the number of internal stages as small as possible (cf. Remark 2), we decompose Ω into two overlapping subdomains $\{\Omega_k\}_{k=1}^2$. In turn, each subdomain is partitioned into $m_k = 2$ disjoint connected components $\{\Omega_{kl}\}_{l=1}^2$, for $k = 1, 2$. To this end, we denote $I = (0,1)$ and consider the intervals where ε is chosen to be $\frac{1}{16}$. Note that the overlapping size takes a value of $\xi = 2\varepsilon = \frac{1}{8}$. The corresponding subdomains are then constructed as follows

$$\Omega_1 \equiv I_1 \times I, \qquad \Omega_2 \equiv I_2 \times I.$$

Following [19], we next define a piecewise smooth partition of unity in accordance with (52). For that purpose, we first introduce the functions

$$w_1(\mathbf{x}) = \begin{cases} 1, & \text{if } x = 0, \\ \sin(\frac{\pi x}{1/4+\varepsilon}), & \text{if } x \in (0, \frac{1}{4}+\varepsilon), \\ \sin(\frac{\pi(x-1/2+\varepsilon)}{1/4+\xi}), & \text{if } x \in (\frac{1}{2}-\varepsilon, \frac{3}{4}+\varepsilon), \\ 0, & \text{otherwise}, \end{cases} \tag{87}$$

and

$$w_2(\mathbf{x}) = \begin{cases} \sin(\frac{\pi(x-1/4+\varepsilon)}{1/4+\xi}), & \text{if } x \in (\frac{1}{4}-\varepsilon, \frac{1}{2}+\varepsilon), \\ \sin(\frac{\pi(x-3/4+\varepsilon)}{1/4+\varepsilon}), & \text{if } x \in (\frac{3}{4}-\varepsilon, 1), \\ 1, & \text{if } x = 1, \\ 0, & \text{otherwise}, \end{cases} \tag{88}$$

and subsequently define $\rho_1(\mathbf{x})$ and $\rho_2(\mathbf{x})$ in $\overline{\Omega}$ by normalizing the previous expressions, i.e.,

$$\rho_k(\mathbf{x}) = \frac{w_k(\mathbf{x})}{w_1(\mathbf{x}) + w_2(\mathbf{x})}, \quad \text{for } k = 1, 2. \tag{89}$$

Using this partition of unity, we consider the splittings $A_h = \sum_{k=1}^2 A_{h,k}$ and $L_h = \sum_{k=1}^2 L_{h,k}$, for the discrete diffusion operator and the semidiscrete source/sink term, respectively. Both $A_{h,k}$ and $L_{h,k}$ are defined in the spirit of Section 5.1. Such splittings are then combined with the two-level Peaceman–Rachford time integration formula in order to obtain a fully discrete scheme for the pressures of the form (65). In this case, the linear system to solve at each implicit internal stage is reduced to a set of two uncoupled subsystems associated to the corresponding disjoint components $\{\Omega_{kl}\}_{l=1}^2$, for $k = 1, 2$,

Table 1
Global errors and numerical orders of convergence in space on the smooth mesh ($\tau = 5\text{E}{-}05$; $h_0 = 2^{-4}$; $\varepsilon = \frac{1}{16}$).

Symmetric method								
h	$\|p - p_h\|_{\ell^\infty(L^2)}$		$\|r_h p - P_h\|_{\ell^\infty(\ell^2)}$		$\|\Pi_h \mathbf{u} - \mathbf{u}_h\|_{\ell^\infty(L^2)}$		$\|\mathbf{u} - \mathbf{u}_h\|_{\ell^\infty(\mathcal{F}_h)}$	
h_0	3.53E−01	–	1.26E−01	–	1.25E+01	–	1.73E+01	–
$h_0/2$	1.68E−01	1.07	3.19E−02	1.98	6.33E+00	0.99	8.88E+00	0.96
$h_0/2^2$	8.30E−02	1.02	8.04E−03	1.99	3.17E+00	1.00	4.48E+00	0.99
$h_0/2^3$	4.14E−02	1.00	2.02E−03	1.99	1.59E+00	1.00	2.24E+00	1.00
$h_0/2^4$	2.08E−02	0.99	5.03E−04	2.01	8.02E−01	0.99	1.11E+00	1.01
Non-symmetric method								
h	$\|p - p_h\|_{\ell^\infty(L^2)}$		$\|r_h p - P_h\|_{\ell^\infty(\ell^2)}$		$\|\Pi_h \mathbf{u} - \mathbf{u}_h\|_{\ell^\infty(L^2)}$		$\|\mathbf{u} - \mathbf{u}_h\|_{\ell^\infty(\mathcal{F}_h)}$	
h_0	3.53E−01	–	1.26E−01	–	1.26E+01	–	1.73E+01	–
$h_0/2$	1.68E−01	1.07	3.20E−02	1.98	6.33E+00	0.99	8.88E+00	0.96
$h_0/2^2$	8.30E−02	1.02	8.04E−03	1.99	3.17E+00	1.00	4.48E+00	0.99
$h_0/2^3$	4.14E−02	1.00	2.02E−03	1.99	1.59E+00	1.00	2.24E+00	1.00
$h_0/2^4$	2.08E−02	0.99	5.03E−04	2.01	8.02E−01	0.99	1.11E+00	1.01

which can be readily solved in parallel. The extension to a higher number of disjoint connected components is addressed below. Regarding the flux variable, we use the fully discrete counterpart of the expression (16) to compute U_h^n in terms of P_h^n at each time step.

Let us now test the convergence of both the symmetric and non-symmetric MFMFE–FSRK$_m$ methods on all three types of meshes. To this end, we consider a sufficiently small fixed time step $\tau = 5\text{E}{-}05$ in order to produce a negligible contribution of the time discretization to the global error. Both the pressure and velocity errors are computed by combining the ℓ^∞-norm in time with various norms in space. In particular, with an abuse of notation, the pressure errors are defined to be

$$\|r_h p - P_h\|_{\ell^\infty(\ell^2)} = \max_{0 \leqslant n \leqslant N_T} \left\| r_h p(t_{n+1}) - P_h^{n+1} \right\|_{\ell^2},$$

and $\|p - p_h\|_{\ell^\infty(L^2)}$ as given by (86). Note that the integral involved in the last expression is approximated element-wise by a 9-point Gaussian quadrature formula. As for the velocity errors, we consider the following expressions

$$\|\Pi \mathbf{u} - \mathbf{u}_h\|_{\ell^\infty(L^2)} = \max_{0 \leqslant n \leqslant N_T} \left\| \Pi \mathbf{u}(t_{n+1}) - \mathbf{u}_h^{n+1} \right\|, \tag{90}$$

$$\|\mathbf{u} - \mathbf{u}_h\|_{\ell^\infty(\mathcal{F}_h)} = \max_{0 \leqslant n \leqslant N_T} \left\| \mathbf{u}(t_{n+1}) - \mathbf{u}_h^{n+1} \right\|_{\mathcal{F}_h}, \tag{91}$$

where $\mathbf{u}_h^{n+1}$ is the element of V_h defined, at each element E, as the Piola transform of a certain function $\hat{\mathbf{v}} \in \hat{V}(\hat{E})$. In particular, the eight degrees of freedom of such $\hat{\mathbf{v}}$ (i.e., the values of $\hat{\mathbf{v}} \cdot \hat{\mathbf{n}}_{\hat{e}}$ at the vertices of each edge $\hat{e} \subset \partial \hat{E}$) are given by the corresponding eight components of the vector U_h^{n+1}. In this case, the integral involved in (90) is approximated by the trapezoidal rule, while that in (91) is computed by a high-order Gaussian quadrature formula.

In Table 1, we show the numerical results obtained for h^2-parallelogram meshes. First-order convergence is observed for both the pressure and velocity variables in the symmetric and non-symmetric MFMFE–FSRK$_m$ methods. In addition, second-order superconvergence is obtained for the pressure at the cell centers. Note that, since $\|r_h p - \bar{p}_h\|_{\ell^2} \leqslant Ch^2$, the convergence behavior of the pressure errors is in accordance with the estimates derived in Remark 4. In turn, the first-order convergence for the flux is consistent with the error estimates derived for the semidiscrete scheme. The results obtained for the family of h-perturbed meshes are similar and can be seen in Table 2. Finally, Table 3 contains the global errors and numerical orders of convergence in space for the randomly perturbed grids with perturbations of size $\mathcal{O}(h)$. On these highly distorted grids, the convergence for both pressures and velocities is preserved by the non-symmetric scheme and deteriorates if the symmetric method is used.

In the remaining of this subsection, we study the convergence in time and scalability of the symmetric MFMFE–FSRK$_m$ method, and the influence of the overlapping size on the accuracy of the splitting technique. For that purpose, we consider the h-perturbed mesh displayed on Fig. 4 and assume the spatial domain Ω to be decomposed into two subdomains $\{\Omega_k\}_{k=1}^2$, each containing an increasing number q of disjoint connected components $\{\Omega_{kl}\}_{l=1}^q$, for $k = 1, 2$. Fig. 6 shows the type of decomposition under consideration. In this representation, the internal boundaries of the disjoint components belonging to Ω_1 and Ω_2 are depicted by dotted and dashed lines, respectively. Accordingly, the partition of unity consists of two piecewise smooth functions $\{\rho_k(\mathbf{x})\}_{k=1}^2$ as introduced in (89). Note that, in this case, the expressions (87) and (88) must be suitably redefined for each chosen value of q. Using the splittings $\{A_{h,k}\}_{k=1}^2$ and $\{L_{h,k}\}_{k=1}^2$, the linear system to solve at the kth internal stage is a collection of q uncoupled subsystems associated to the components $\{\Omega_{kl}\}_{l=1}^q$, for $k = 1, 2$. Thus, the algorithm can be implemented on q parallel processors, each of which will solve the corresponding subsystem in a specific component.

In order to study the convergence behavior in time of the scheme, we fix $h = 2^{-8}$ so that the error in space is negligible. Table 4 shows the global errors and numerical orders of convergence in time for $\|r_h p - P_h\|_{\ell^\infty(\ell^2)}$. In accordance with the

Table 2
Global errors and numerical orders of convergence in space on the h-perturbed mesh ($\tau = 5\text{E}{-}05$; $h_0 = 2^{-4}$; $\varepsilon = \frac{1}{16}$).

Symmetric method								
h	$\|p - p_h\|_{\ell^\infty(L^2)}$		$\|r_h p - P_h\|_{\ell^\infty(\ell^2)}$		$\|\Pi_h \mathbf{u} - \mathbf{u}_h\|_{\ell^\infty(L^2)}$		$\|\mathbf{u} - \mathbf{u}_h\|_{\ell^\infty(\mathcal{F}_h)}$	
h_0	3.67E−01	–	1.23E−01	–	1.66E+01	–	1.94E+01	–
$h_0/2$	1.77E−01	1.05	2.88E−02	2.09	8.39E+00	0.98	1.02E+01	0.93
$h_0/2^2$	8.76E−02	1.01	6.98E−03	2.04	4.20E+00	1.00	5.15E+00	0.99
$h_0/2^3$	4.37E−02	1.00	1.73E−03	2.01	2.10E+00	1.00	2.59E+00	0.99
$h_0/2^4$	2.21E−02	0.98	4.33E−04	2.00	1.06E+00	0.99	1.29E+00	1.01
Non-symmetric method								
h	$\|p - p_h\|_{\ell^\infty(L^2)}$		$\|r_h p - P_h\|_{\ell^\infty(\ell^2)}$		$\|\Pi_h \mathbf{u} - \mathbf{u}_h\|_{\ell^\infty(L^2)}$		$\|\mathbf{u} - \mathbf{u}_h\|_{\ell^\infty(\mathcal{F}_h)}$	
h_0	3.64E−01	–	1.24E−01	–	1.66E+01	–	1.95E+01	–
$h_0/2$	1.76E−01	1.05	2.86E−02	2.12	8.39E+00	0.98	1.02E+01	0.93
$h_0/2^2$	8.75E−02	1.01	6.85E−03	2.06	4.20E+00	1.00	5.16E+00	0.98
$h_0/2^3$	4.37E−02	1.00	1.69E−03	2.02	2.10E+00	1.00	2.59E+00	0.99
$h_0/2^4$	2.21E−02	0.98	4.21E−04	2.01	1.06E+00	0.99	1.29E+00	1.01

Table 3
Global errors and numerical orders of convergence in space on the randomly h-perturbed mesh ($\tau = 5\text{E}{-}05$; $h_0 = 2^{-4}$; $\varepsilon = \frac{1}{16}$).

Symmetric method								
h	$\|p - p_h\|_{\ell^\infty(L^2)}$		$\|r_h p - P_h\|_{\ell^\infty(\ell^2)}$		$\|\Pi_h \mathbf{u} - \mathbf{u}_h\|_{\ell^\infty(L^2)}$		$\|\mathbf{u} - \mathbf{u}_h\|_{\ell^\infty(\mathcal{F}_h)}$	
h_0	3.47E−01	–	1.22E−01	–	1.25E+01	–	1.73E+01	–
$h_0/2$	1.67E−01	1.06	3.62E−02	1.75	6.44E+00	0.96	8.80E+00	0.98
$h_0/2^2$	8.31E−02	1.01	1.78E−02	1.02	3.91E+00	0.72	5.92E+00	0.57
$h_0/2^3$	4.33E−02	0.94	1.52E−02	0.23	2.90E+00	0.42	5.03E+00	0.24
$h_0/2^4$	2.52E−02	0.78	1.50E−02	0.02	2.82E+00	0.04	5.07E+00	< 0
Non-symmetric method								
h	$\|p - p_h\|_{\ell^\infty(L^2)}$		$\|r_h p - P_h\|_{\ell^\infty(\ell^2)}$		$\|\Pi_h \mathbf{u} - \mathbf{u}_h\|_{\ell^\infty(L^2)}$		$\|\mathbf{u} - \mathbf{u}_h\|_{\ell^\infty(\mathcal{F}_h)}$	
h_0	3.52E−01	–	1.38E−01	–	1.24E+01	–	1.70E+01	–
$h_0/2$	1.66E−01	1.08	2.97E−02	2.22	6.33E+00	0.97	8.78E+00	0.95
$h_0/2^2$	8.21E−02	1.02	7.71E−03	1.95	3.20E+00	0.98	4.45E+00	0.98
$h_0/2^3$	4.08E−02	1.01	1.86E−03	2.05	1.60E+00	1.00	2.23E+00	1.00
$h_0/2^4$	2.04E−02	1.00	4.67E−04	1.99	8.03E−01	0.99	1.15E+00	0.96

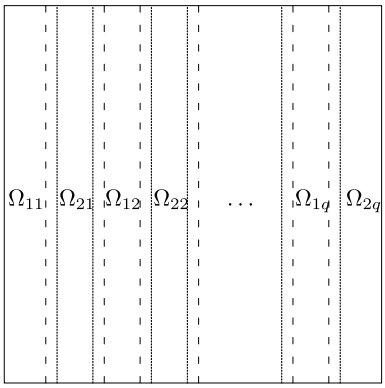

Fig. 6. Decomposition of Ω into two subdomains Ω_1 and Ω_2, each consisting of q disjoint connected components $\{\Omega_{1l}\}_{l=1}^q$ and $\{\Omega_{2l}\}_{l=1}^q$. The internal boundaries of such components belonging to Ω_1 and Ω_2 are represented by dotted and dashed lines, respectively.

theory, for any given q, the method is second-order convergent and unconditionally stable. Although not reported in the table, similar results are obtained for $\|p - p_h\|_{\ell^\infty(L^2)}$.

In Table 5, we study the effect of a reduction in the overlapping size ξ on the accuracy of the splitting technique. For a specific number of processors, the global error $\|r_h p - P_h\|_{\ell^\infty(\ell^2)}$ increases as the overlapping size is reduced. This is due to the fact that the error constant depends on negative powers of the overlapping size. According to the experimental data shown in the table, such a constant doubles as the value of ε is halved. Similar results concerning the influence of the overlapping size on the global error of domain decomposition splitting schemes are reported in [19].

To conclude, we perform a scalability test on a shared-memory machine with 48 GB of RAM that runs CentOS 6.3 and has 8 Intel(R) Xeon(R) CPU E5607 2.27 GHz processors. For an increasing number q of processors, Table 6 displays the communication time $\mathtt{T_{comm}}$, the computation time $\mathtt{T_{comp}}$, and the total execution time $\mathtt{T_{total}}$ (all three measured in

Table 4
Global errors and numerical orders of convergence in time for the symmetric method on the h-perturbed mesh ($h = 2^{-8}$; $\tau_0 = 1\text{E}{-}02$; $\varepsilon = \frac{1}{80}$).

q	2		4		8	
τ	$\|r_h p - P_h\|_{\ell^\infty(\ell^2)}$		$\|r_h p - P_h\|_{\ell^\infty(\ell^2)}$		$\|r_h p - P_h\|_{\ell^\infty(\ell^2)}$	
τ_0	1.46E−01	–	1.36E−01	–	2.24E−01	–
$\tau_0/2^{1/2}$	7.00E−02	2.12	6.98E−02	1.92	1.16E−01	1.90
$\tau_0/2$	3.27E−02	2.20	3.54E−02	1.96	5.80E−02	2.00
$\tau_0/2^{3/2}$	1.69E−02	1.90	1.78E−02	1.98	2.89E−02	2.01
$\tau_0/2^2$	8.83E−03	1.87	8.88E−03	2.01	1.45E−02	1.99

Table 5
Effect of the overlapping size on the accuracy of the method. Global errors for the symmetric method on the h-perturbed mesh ($h = 2^{-9}$; $\tau = 5E{-}03$; $\varepsilon_0 = \frac{1}{80}$).

q	2	4	8
ε	$\|r_h p - P_h\|_{\ell^\infty(\ell^2)}$	$\|r_h p - P_h\|_{\ell^\infty(\ell^2)}$	$\|r_h p - P_h\|_{\ell^\infty(\ell^2)}$
ε_0	3.76E−02	4.07E−02	6.56E−02
$\varepsilon_0/2^{1/2}$	5.46E−02	5.41E−02	9.25E−02
$\varepsilon_0/2$	7.03E−02	6.67E−02	1.16E−01
$\varepsilon_0/2^{3/2}$	9.59E−02	9.22E−02	1.53E−01
$\varepsilon_0/2^2$	1.47E−01	1.33E−02	2.23E−01

Table 6
Scalability test for the symmetric method on the h-perturbed mesh. Component size indicates the number of grid points on each connected component, with $\alpha \in \{\lceil \frac{\varepsilon}{h} \rceil, 2\lceil \frac{\varepsilon}{h} \rceil\} = \{7, 14\}$ ($h = 2^{-9}$; $\tau = 5\text{E}{-}03$; $\varepsilon = \frac{1}{80}$).

q	Component size	$\mathtt{T_{comm}}$	$\mathtt{T_{comp}}$	$\mathtt{T_{total}}$	$S(q)$	$E(q)$	$S^*(q)$
1	$(256+\alpha)\times 512$	0.00E+00	1.45E+03	1.45E+03	1.00	100.00	1.00
2	$(128+\alpha)\times 512$	6.11E+01	7.23E+02	7.84E+02	1.85	92.50	1.85
4	$(64+\alpha)\times 512$	9.76E+01	3.85E+02	4.82E+02	3.01	75.25	3.23
8	$(32+\alpha)\times 512$	1.03E+02	2.55E+02	3.58E+02	4.05	50.63	5.13

seconds), together with the parallel speedup $S(q)$ and the efficiency $E(q)$. The last column contains the maximum theoretical speedup $S^*(q)$ predicted by Amdahl's law (to be defined below). Note that the value $q = 1$ represents the implementation of the serial algorithm on a single processor. As q grows from 1 to 8 by powers of 2, the increase in $\mathtt{T_{comm}}$ is observed to be slower than the decrease in $\mathtt{T_{comp}}$. This results in a global reduction of $\mathtt{T_{total}}$ throughout the experiment. In order to measure the reduction rate, we define the speedup $S(q)$ as the ratio of the runtime of the serial program to that of the parallel program with q processors. Thus, the efficiency is defined to be $E(q) = S(q)/q \times 100$. Remarkably, the speedup increases at a slower rate each time the number of processors is doubled. As a result, the parallel efficiency keeps on diminishing as q gets a larger value. This behavior is predicted by Amdahl's law, which establishes that, for a problem of fixed size, the maximum speedup is given by

$$S^*(q) = \frac{1}{(1-F) + \frac{F}{q}}. \tag{92}$$

Here, F is the fraction of time spent by a serial processor on parts of the algorithm that can be done in parallel. In this case, using the MPI profiling tools, we estimate a value of $F = 0.92$. Hence, the computed speedups displayed on Table 6 are in accordance with the theoretical values provided by the expression (92).

7.2. Flow through a porous medium with discontinuous permeability

Let us now consider a numerical example of single-phase flow through a porous medium containing a low-permeability streak. Stationary versions of this problem are solved using alternative spatial discretizations in [56–58]. In particular, we consider problem (1) posed on the unit square, with $T = 2$, $\Gamma_D = \{0, 1\} \times (0, 1)$, $\Gamma_N = [0, 1] \times \{0, 1\}$, $f(\mathbf{x}, t) = 0$ and $p_0(\mathbf{x}) = 1 - x$. Pressure is specified to be equal to 1 on the boundary $\{0\} \times (0, 1)$ and equal to 0 on $\{1\} \times (0, 1)$. In turn, zero flux is set on Γ_N.

The flow domain contains a low-permeability region which is delimited by two curves. The top curve is chosen to be an arc of a circle with center at $(0.1, -0.4)$ and radius equal to 1.2, while the bottom curve is an arc of a circle with the same center and radius equal to 1.1. The permeability throughout the domain is uniform and isotropic ($K = I_2$), except in the low-permeability streak. In this region, it is such that the parallel component to the local streak orientation ($K_\parallel$) is equal to 0.1, and the normal component to the local streak orientation ($K_\perp$) is equal to 0.001. In the x–y coordinate system, the permeability within the streak is a full tensor, whose components are given by

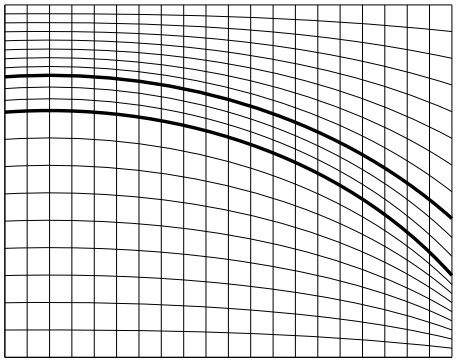

Fig. 7. Geometry of the flow domain and logically rectangular grid.

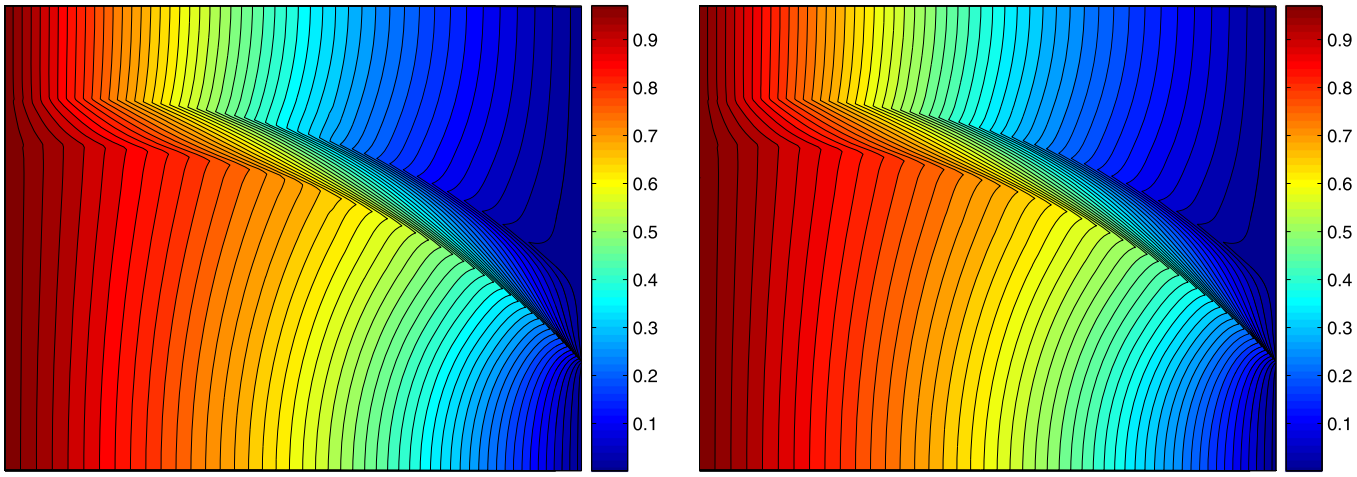

Fig. 8. Pressure distributions for the MFMFE–FSRK$_m$ method (left) and for the MFMFE–TR method (right).

$$K_{xx} = K_{\parallel}\cos^2\phi + K_{\perp}\sin^2\phi,$$
$$K_{xy} = (K_{\parallel} - K_{\perp})\cos\phi\sin\phi,$$
$$K_{yy} = K_{\parallel}\sin^2\phi + K_{\perp}\cos^2\phi.$$

Here, $\phi = \phi(x, y)$ is the rotation angle of the orthogonal coordinate system in which K is a diagonal tensor with elements $K_{\parallel}$ and $K_{\perp}$. More specifically,

$$\sin\phi = -\frac{\hat{x}}{\sqrt{\hat{x}^2 + \hat{y}^2}}, \qquad \cos\phi = \frac{\hat{y}}{\sqrt{\hat{x}^2 + \hat{y}^2}},$$

where $\hat{x} = x - 0.1$ and $\hat{y} = y + 0.4$.

In order to solve this problem, we consider the MFMFE–FSRK$_m$ method (65), with $m = 2$ subdomains and $m_k = 1$ connected component per subdomain. In particular, we define $\Omega_1 = (0, \frac{9}{16}) \times (0, 1)$ and $\Omega_2 = (\frac{7}{16}, 1) \times (0, 1)$. Moreover, a combination of the MFMFE scheme with a classical time integration formula – namely, the trapezoidal rule (TR) – is used. This numerical example permits us to test the behavior of the spatial discretization method to accurately solve problems containing irregularly shaped strata and abrupt variations in permeability. In addition, it provides a qualitative comparison between the proposed time-splitting approach and a standard time integrator in terms of accuracy of the numerical solution.

Fig. 7 shows the geometry of the flow domain and the type of logically rectangular grid used in the discretization. Observe that the grid is adapted to the geometry of the low-permeability streak, depicted in the figure by bold curves. In Fig. 8, we display contour plots of the pressure distribution obtained with both discretizations once the stationary state is reached. Both methods consider the quadrilateral mesh shown in Fig. 7, with 200×200 elements, and a time step $\tau = 5\text{E}{-}03$. Note the effect of the low-permeability streak on the pressure distribution. As it can be observed, the numerical solution resulting from the MFMFE–FSRK$_m$ scheme is qualitatively similar to that obtained with the MFMFE–TR method. Finally, Fig. 9 shows the velocity field obtained with both discretizations at the stationary state. As usual, the length of the arrows is proportional to the module of the vectors. In this case, a quadrilateral mesh with 20×20 elements and a time step $\tau = 5\text{E}{-}03$ are considered. Once again, the results are comparable for both approaches. As expected from the physical configuration, no flow enters the streak, so these results are also in accordance with those obtained in [56–58].

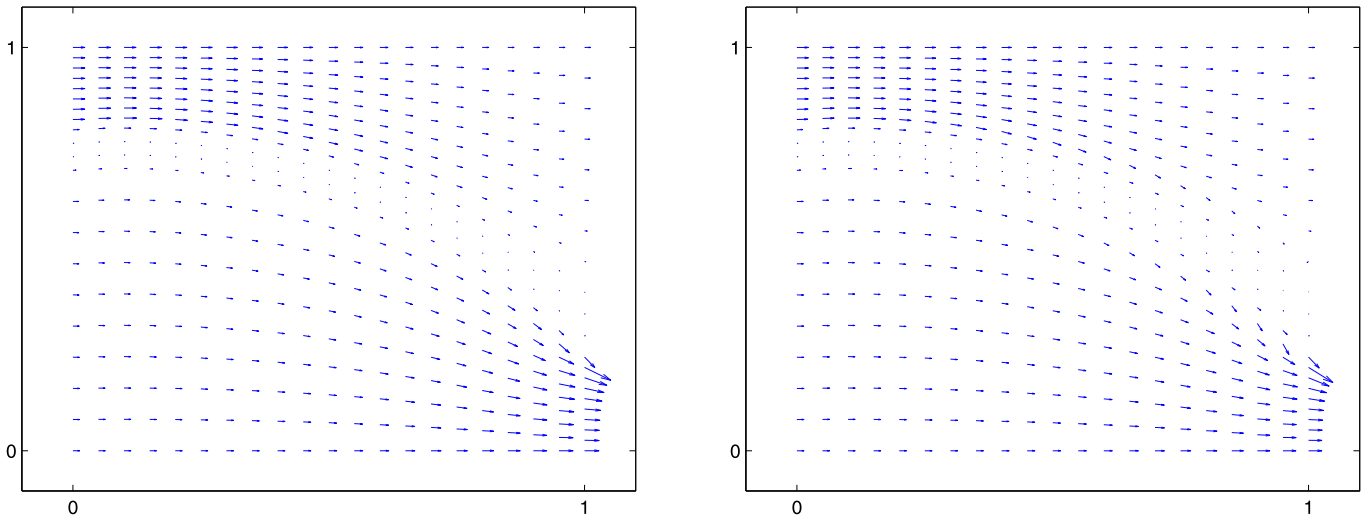

Fig. 9. Velocity fields for the MFMFE–FSRK$_m$ method (left) and for the MFMFE–TR method (right).

Significantly, the numerical solutions obtained for a different number m of subdomains and/or a different number m_k of disjoint connected components per subdomain are similar to those represented on the left-hand side of Figs. 8 and 9.

Acknowledgements

The first two authors gratefully acknowledge the hospitality of the Department of Mathematics at the University of Pittsburgh, where this research was partly carried out. The work of the first two authors was partially supported by MICINN grant MTM2010-21037. The third author was partially supported by NSF grant DMS 1115856 and DOE grant DE-FG02-04ER25618.

References

[1] M.F. Wheeler, I. Yotov, A multipoint flux mixed finite element method, SIAM J. Numer. Anal. 44 (2006) 2082–2106.
[2] R.A. Klausen, R. Winther, Convergence of multipoint flux approximations on quadrilateral grids, Numer. Methods Partial Differ. Equ. 22 (2006) 1438–1454.
[3] R.A. Klausen, R. Winther, Robust convergence of multi point flux approximation on rough grids, Numer. Math. 104 (2006) 317–337.
[4] I. Aavatsmark, G.T. Eigestad, R.A. Klausen, M.F. Wheeler, I. Yotov, Convergence of a symmetric MPFA method on quadrilateral grids, Comput. Geosci. 11 (2007) 335–345.
[5] R. Ingram, M.F. Wheeler, I. Yotov, A multipoint flux mixed finite element method on hexahedra, SIAM J. Numer. Anal. 48 (2010) 1281–1312.
[6] M.F. Wheeler, G. Xue, I. Yotov, A multiscale mortar multipoint flux mixed finite element method, Math. Model. Numer. Anal. 46 (2012) 759–796.
[7] M.F. Wheeler, G. Xue, I. Yotov, A multipoint flux mixed finite element method on distorted quadrilaterals and hexahedra, Numer. Math. 121 (2012) 165–204.
[8] A. Arrarás, L. Portero, J.C. Jorge, Convergence of fractional step mimetic finite difference discretizations for semilinear parabolic problems, Appl. Numer. Math. 60 (2010) 473–485.
[9] A. Arrarás, Mimetic fractional step methods for parabolic problems, PhD thesis, Universidad Carlos III de Madrid, Madrid, 2011.
[10] I. Aavatsmark, An introduction to multipoint flux approximations for quadrilateral grids, Comput. Geosci. 6 (2002) 405–432.
[11] I. Aavatsmark, T. Barkve, O. Bøe, T. Mannseth, Discretization on unstructured grids for inhomogeneous, anisotropic media. Part II: Discussion and numerical results, SIAM J. Sci. Comput. 19 (1998) 1717–1736.
[12] M.G. Edwards, C.F. Rogers, Finite volume discretization with imposed flux continuity for the general tensor pressure equation, Comput. Geosci. 2 (1998) 259–290.
[13] M.G. Edwards, Unstructured, control-volume distributed, full-tensor finite-volume schemes with flow based grids, Comput. Geosci. 6 (2002) 433–452.
[14] F. Brezzi, J. Douglas Jr., L.D. Marini, Two families of mixed finite elements for second order elliptic problems, Numer. Math. 47 (1985) 217–235.
[15] F. Brezzi, J. Douglas Jr., R. Durán, M. Fortin, Mixed finite elements for second order elliptic problems in three variables, Numer. Math. 51 (1987) 237–250.
[16] I. Faragó, A. Havasiy, Operator Splittings and Their Applications, Math. Res. Dev., Nova Science Publishers, Inc., New York, 2009.
[17] P.N. Vabishchevich, Difference schemes with domain decomposition for solving non-stationary problems, USSR Comput. Math. Math. Phys. 29 (1989) 155–160.
[18] P.N. Vabishchevich, Parallel domain decomposition algorithms for time-dependent problems of mathematical physics, in: I.T. Dimov, B. Sendov, P.S. Vassilevski (Eds.), Advances in Numerical Methods and Applications, World Scientific, River Edge, 1994, pp. 293–299.
[19] T.P. Mathew, P.L. Polyakov, G. Russo, J. Wang, Domain decomposition operator splittings for the solution of parabolic equations, SIAM J. Sci. Comput. 19 (1998) 912–932.
[20] L. Portero, B. Bujanda, J.C. Jorge, A combined fractional step domain decomposition method for the numerical integration of parabolic problems, in: R. Wyrzykowski, J. Dongarra, M. Paprzycki, J. Wasniewski (Eds.), Parallel Processing and Applied Mathematics, in: Lect. Notes Comput. Sci., vol. 3019, Springer-Verlag, Berlin, 2004, pp. 1034–1041.
[21] P.N. Vabishchevich, Domain decomposition methods with overlapping subdomains for the time-dependent problems of mathematical physics, Comput. Methods Appl. Math. 8 (2008) 393–405.
[22] A.A. Samarskiĭ, P.P. Matus, P.N. Vabishchevich, Difference Schemes with Operator Factors, Math. Appl., vol. 546, Kluwer Academic Publishers, Dordrecht, 2002.
[23] T.P.A. Mathew, Domain Decomposition Methods for the Numerical Solution of Partial Differential Equations, Lect. Notes Comput. Sci. Eng., vol. 61, Springer-Verlag, Berlin, 2008.

[24] B. Bujanda, J.C. Jorge, Fractional step Runge–Kutta methods for time dependent coefficient parabolic problems, Appl. Numer. Math. 45 (2003) 99–122.
[25] L. Portero, J.C. Jorge, A generalization of Peaceman–Rachford fractional step method, J. Comput. Appl. Math. 189 (2006) 676–688.
[26] D.W. Peaceman, H.H. Rachford Jr., The numerical solution of parabolic and elliptic differential equations, J. Soc. Ind. Appl. Math. 3 (1955) 28–41.
[27] W.J. Layton, P.J. Rabier, Peaceman–Rachford procedure and domain decomposition for finite element problems, Numer. Linear Algebra Appl. 2 (1995) 363–393.
[28] C. Du, D. Liang, An efficient S-DDM iterative approach for compressible contamination fluid flows in porous media, J. Comput. Phys. 229 (2010) 4501–4521.
[29] A. Quarteroni, A. Valli, Domain Decomposition Methods for Partial Differential Equations, Numer. Math. Sci. Comput., Oxford University Press, New York, 1999.
[30] W.H. Hundsdorfer, J.G. Verwer, Stability and convergence of the Peaceman–Rachford ADI method for initial-boundary value problems, Math. Comput. 53 (1989) 81–101.
[31] J.M. Thomas, Sur l'analyse numérique des méthods d'éléments finis hybrides et mixtes, PhD thesis, Université Pierre et Marie Curie, Paris, 1977.
[32] F. Brezzi, M. Fortin, Mixed and Hybrid Finite Element Methods, Springer Ser. Comput. Math., vol. 15, Springer-Verlag, New York, 1991.
[33] R.A. Raviart, J.M. Thomas, A mixed finite element method for 2-nd order elliptic problems, in: I. Galligani, E. Magenes (Eds.), Mathematical Aspects of Finite Element Methods, in: Lect. Notes Math., vol. 606, Springer, Berlin, 1977, pp. 292–315.
[34] J.-C. Nédélec, Mixed finite elements in $\mathbb{R}^3$, Numer. Math. 35 (1980) 315–341.
[35] K. Lipnikov, M. Shashkov, I. Yotov, Local flux mimetic finite difference methods, Numer. Math. 112 (2009) 115–152.
[36] M.F. Wheeler, A priori L_2 error estimates for Galerkin approximations to parabolic partial differential equations, SIAM J. Numer. Anal. 10 (1973) 723–759.
[37] R.E. Ewing, R.D. Lazarov, Superconvergence of the mixed finite element approximations of parabolic problems using rectangular finite elements, East-West J. Numer. Math. 1 (1993) 199–212.
[38] V. Thomée, Galerkin Finite Element Methods for Parabolic Problems, Springer Ser. Comput. Math., vol. 25, Springer-Verlag, Berlin, 1997.
[39] G.I. Marchuk, Splitting and alternating direction methods, in: P.G. Ciarlet, J.L. Lions (Eds.), Finite Difference Methods. Part 1. Solution of Equations in $\mathbb{R}^n$. Part 1, in: Handb. Numer. Anal., vol. 1, North-Holland, Amsterdam, 1990, pp. 197–462.
[40] J.G. Verwer, J.M. Sanz-Serna, Convergence of method of lines approximations to partial differential equations, Computing 33 (1984) 297–313.
[41] J.M. Sanz-Serna, J.G. Verwer, W.H. Hundsdorfer, Convergence and order reduction of Runge–Kutta schemes applied to evolutionary problems in partial differential equations, Numer. Math. 50 (1986) 405–418.
[42] J.M. Sanz-Serna, J.G. Verwer, Stability and convergence at the PDE/stiff ODE interface, Appl. Numer. Math. 5 (1989) 117–132.
[43] M. Crouzeix, Sur l'approximation des équations différentielles opérationnelles linéaires par des méthodes de Runge–Kutta, PhD thesis, Université Paris VI, Paris, 1975.
[44] S. Brenner, M. Crouzeix, V. Thomée, Single step methods for inhomogeneous linear differential equations in Banach space, RAIRO. Anal. Numér. 16 (1982) 5–26.
[45] A. Ostermann, M. Roche, Runge–Kutta methods for partial differential equations and fractional orders of convergence, Math. Comput. 59 (1992) 403–420.
[46] C. Lubich, A. Ostermann, Interior estimates for time discretizations of parabolic equations, Appl. Numer. Math. 18 (1995) 241–251.
[47] M.P. Calvo, C. Palencia, Avoiding the order reduction of Runge–Kutta methods for linear initial boundary value problems, Math. Comput. 71 (2002) 1529–1543.
[48] G. Fairweather, A.R. Mitchell, A new computational procedure for A.D.I. methods, SIAM J. Numer. Anal. 4 (1967) 163–170.
[49] B.P. Sommeijer, P.J. van der Houwen, J.G. Verwer, On the treatment of time-dependent boundary conditions in splitting methods for parabolic differential equations, Int. J. Numer. Methods Eng. 17 (1981) 335–346.
[50] I. Alonso-Mallo, B. Cano, J.C. Jorge, Spectral-fractional step Runge–Kutta discretizations for initial boundary value problems with time dependent boundary conditions, Math. Comput. 73 (2004) 1801–1825.
[51] M.G. Edwards, Cross flow tensors and finite volume approximation with deferred correction, Comput. Methods Appl. Mech. Eng. 151 (1998) 143–161.
[52] M.G. Edwards, M-matrix flux splitting for general full tensor discretization operators on structured and unstructured grids, J. Comput. Phys. 160 (2000) 1–28.
[53] M.G. Edwards, Split full tensor discretization operators for general hexahedral grids, SPE J. 9 (2004) 102–108.
[54] D.N. Arnold, D. Boffi, R.S. Falk, Quadrilateral $H(\mathrm{div})$ finite elements, SIAM J. Numer. Anal. 42 (2005) 2429–2451.
[55] D. Boffi, L. Gastaldi, Some remarks on quadrilateral mixed finite elements, Comput. Struct. 87 (2009) 751–757.
[56] L.J. Durlofsky, A triangle based mixed finite element-finite volume technique for modeling two phase flow through porous media, J. Comput. Phys. 105 (1993) 252–266.
[57] L.J. Durlofsky, Accuracy of mixed and control volume finite element approximations to Darcy velocity and related quantities, Water Resour. Res. 30 (1994) 965–973.
[58] J. Hyman, M. Shashkov, S. Steinberg, The numerical solution of diffusion problems in strongly heterogeneous non-isotropic materials, J. Comput. Phys. 132 (1997) 130–148.